Panx1 Ablation Aggravates Oxidative Stress and Cell Death by Altering AMPK/mTOR signaling Pathways and the Composition of Synapses in the Zebrafish.

***Authors**:* Georg S.O. Zoidl[1,3], Nickie Safarian[1,4], Christiane Zoidl[1,2], Steven Connor[1,3], Georg R. Zoidl[1,2,3]

Affiliations: [1] Department of Biology, [2] Department of Psychology, [3] Center for Integrated and Applied Neuroscience (CIAN), York University, [4] Department of Genomics and Genome Biology, Sick Kids Hospital, Toronto, Canada.

Corresponding Author: Georg R. Zoidl, gzoidl@yorku.ca

Graphical Abstract

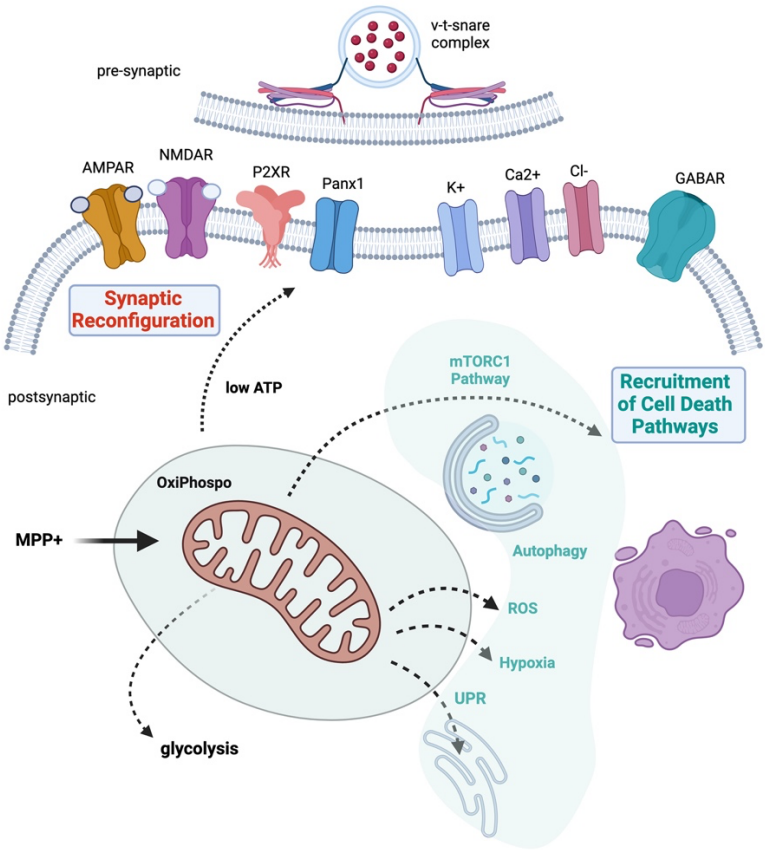

Highlights

- A genetic model was combined with the neurotoxin MPTP to explore the roles of zebrafish Pannexin-1 channels in neurodevelopment under oxidative stress conditions.
- A potential beneficial impact of targeting Panx1a is superseded by synaptic plasticity loss, dysfunctional mitochondrial metabolism, and cell death pathway activation.
- Loss of Panx1a amplifies AMPK/mTORC1 pathway activation of cell death pathways.
- A role of Panx1a as a regulator of energy and synaptic homeostasis was identified.

46 ***Abstract:***

47 Pannexin-1 channels have garnered attention for their implications in neurodevelopment,
48 potentially having a dual role in mediating a delicate balance between cell death and survival.
49 However, a comprehensive understanding of the underlying molecular and cellular mechanisms
50 and Panx1's potential protective functions throughout neurodevelopment remains to be
51 determined. Zebrafish larvae with loss of Pannexin-1a function were subjected to an acute
52 exposure to 1-methyl-4-phenyl-1,2,3,6-tetrahydropyridine (MPTP). Early-life changes in larvae
53 induced by uncoupling of oxidative phosphorylation were investigated by a computational Gene
54 Set Expression Analysis of RNA-seq data and experimental testing of light-stimulated locomotor
55 behavior, cell death, and bioelectrical properties of local field potentials in the ascending visual
56 pathway. A KEGG pathway analysis underscored Panx1a's regulatory influence on
57 neurodevelopment. Targeting Panx1a caused a deregulation of oxidative phosphorylation,
58 glycolysis, reactive oxygen production, hypoxia, unfolded protein response pathways, and
59 reduced extracellular ATP. Further, Panx1a ablation enhanced the transcriptional activation of 5'
60 AMP-activated protein kinase (AMPK) kinase, a cellular energy sensor activated by falling
61 energy status, largely to activate glucose and fatty acid uptake and oxidation when cellular energy
62 is low. The activation of the AMPK pathway in Panx1a knock-out larvae correlated with the
63 stimulation of the mammalian target of rapamycin (mTORC1) pathway that controls cellular
64 metabolism, catabolism, immune responses, autophagy, survival, proliferation, and migration, to
65 maintain cellular homeostasis. The differential expression of mTORC1 pathway genes associated
66 with autophagy, and apoptosis signaling pathways. The resultant cell death was pronounced in
67 the pallium and tectum regions. The loss of cells interrelated with a trans-synaptic a loss of
68 synaptic neurotransmitter receptor and ion channel/transporter expression. Local field potential
69 recordings in the optic tectum and pallium demonstrated that Panx1a's involvement in modulating

local neuronal networks was altered. Collectively, the results shed light on the impacts of acute MPTP treatment on locomotor behavior, transcriptomic shifts, metabolic disturbances, and the pivotal role of Panx1a in cell death. These insights enhance our comprehension of the intricate molecular and cellular mechanisms underpinning neurodevelopment, with implications for potential therapeutic strategies targeting Panx1 channels in autism and Alzheimer's disease.

Keywords:

Pannexin, synapse, AMPK/mTORC1 pathway, autophagy, RNA-seq, behavior, local-field potential, MPTP, zebrafish, gene-editing.

Introduction

Pannexin 1 (Panx1) forms channels with significant roles in neurodevelopment, synapse function, and cellular signaling and communication between neurons and glial cells. The multifaceted roles of this channel in brain development encompasses structural aspects of neuronal and synaptic function such as the formation and stabilization of dendritic spines, which are essential for synaptic connectivity and plasticity. The absence of Panx1 leads to higher dendritic spine densities and more intricate neuronal networks, indicating that Panx1 regulates the dynamics of dendritic and spiny protrusions, thus influencing the overall architecture of neuronal networks.

In addition to structural roles, Panx1 channels are key modulators of synaptic transmission and plasticity. For example, Panx1 knockout (Panx1$^{-/-}$) mice exhibit enhanced excitability and more complex dendritic branching. These changes are linked to increased actin polymerization and imbalances in Rho GTPase activities, suggesting that Panx1 interacts with the

94 cytoskeleton to regulate synapse function. Panx1 also regulates long-term potentiation (LTP) and
95 long-term depression (LTD) at hippocampal synapses, processes critical for learning and
96 memory. Panx1$^{-/-}$ mice display deficiencies in long-term spatial reference memory, implicating
97 Panx1 in memory consolidation.

98 Panx1's role in neuron-glia interactions and ATP release is crucial for neuro-
99 developmental processes. It is vital for neural stem cell survival, neuronal maturation, and
100 synaptic plasticity. Furthermore, Panx1's role in ATP release and purinergic signaling is crucial
101 for neurodevelopmental processes, including NPC proliferation and migration, which are
102 foundational for establishing synchronized neuronal networks and preventing pathological
103 conditions such as seizures. A recently published Panx1 interactome reveals associations with
104 proteins involved in synaptic function and neurodevelopmental and neurodegenerative diseases,
105 indicating a broader role in synaptic homeostasis and network functions.

106 Overall, Panx1 has emerged as a critical player in brain development, influencing synaptic
107 formation, stability, plasticity, neuron-glia communication, and neuronal network formation. The
108 functions extend to maintaining synaptic stability, contributing to memory and learning, and
109 participating in signaling pathways essential for brain function. While Panx1's involvement in
110 neuronal development and system circuitry formation is documented, the underlying molecular
111 and cellular mechanisms of how these channels influence embryogenesis and early postnatal
112 development await a more detailed characterization.

113 Zebrafish larvae are an established model for studying cell signaling and communication
114 during embryogenesis and early postnatal development. The extra-corporal embryogenesis ends
115 with the hatching of transparent larvae at three days post fertilization (3dpf). At six days post
116 fertilization (6dpf), during post-embryonic development, extensive cellular communication drives

117 growth, differentiation, and responses to environmental cues. The rapid development of
118 behaviors signifies the maturation of functional neuronal networks.

119 We were specifically interested in the role of dopaminergic neurons during this period due
120 to their extensive roles in developmental processes regulating the formation and maturation of
121 neural circuits, influencing behaviors, and cognitive functions. Furthermore, imbalances of
122 dopaminergic signaling potentially lead to conditions such as autism, attention-
123 deficit/hyperactivity disorder (ADHD), and schizophrenia, or present as a risk factor for
124 neurodegenerative disorders (NDDs) like Parkinson's disease (PD).

125 We have previously identified in 6dpf zebrafish larvae a neurodevelopmental deficit when
126 ablation of Panx1a, the ortholog of mammalian Panx1, caused visuomotor deficiency linked to
127 changes in dopaminergic signaling. To get insight into the roles of Panx1 in dopaminergic
128 signaling, we targeted dopaminergic neurons by inducing rapid neurotoxicity in six-day-old
129 Tubingen Longfin (TL) larvae with 1-methyl-4-phenyl-1,2,3,6-tetrahydropyridine (MPTP).
130 MPTP crosses the blood-brain barrier and is converted to the toxic MPP+ by the mitochondrial
131 monoamine oxidase (Mao-B). MPP+ is taken up by the dopamine transporter (DAT) expressed
132 by dopaminergic neurons, inactivating the mitochondrial respiratory complex I. By disrupting
133 dopaminergic signaling in a Panx1 knockout zebrafish line (Panx1a$^{-/-}$) we tested the hypothesis
134 that Panx1a acts as a regulator linking mitochondrial health with synapse function. The
135 computational analysis of RNA-seq data showed that a four-hour treatment in TL (Panx1a$^{+/+}$) and
136 Panx1a$^{-/-}$ larvae was sufficient to initiate transcriptome-wide expression changes indicating
137 metabolic dysfunction, impaired proteostasis, differential expression of genes involved in
138 neurodevelopmental and neurodegenerative disorders, and cell death. MPTP also caused a dose-
139 dependent reduction in swimming behavior. By comparing MPTP effects on Panx1a$^{-/-}$ and
140 Panx1a$^{+/+}$ strains, RNA-seq, and Gene Set Expression Analysis (GSEA), we found that Panx1a

141 ablation altered the expression of hallmark genes for autism, Alzheimer's, and Parkinson's
142 disease, reducing the expression of zebrafish orthologs of mammalian Shank, alpha-Synuclein,
143 and Tau proteins. In contrast, Panx1a ablation reduced extracellular ATP, and enhanced
144 differential expression of cell signaling pathways regulating oxidative phosphorylation, cell
145 death, lipid synthesis, ROS signaling, and intracellular quality controls. Ablation of Panx1a also
146 altered synapse molecular composition, impairing synaptic function, demonstrated *in vivo* by
147 recording changes to local field potentials. Alterations of in the optic tectum (OT) and dorso-
148 medial (DM) pallium corroborated neuronal network dysfunctions.

149 In summary, this study's findings suggest an intricate relationship between Panx1a,
150 synapses, and mitochondrial health underscoring the importance of maintaining mitochondrial
151 integrity and balanced dopamine signaling for optimal neurodevelopment. The animal model
152 introduced here can provide insights into potential therapeutic targets for mitigating the impact of
153 these disorders on neurodevelopmental health.

154

155 **Materials and Methods**

156 **Zebrafish lines.** Zebrafish (*Danio Rerio*) of strain Tubingen long fin (TL) were maintained in
157 groups with mixed sex in a recirculation system (Aquaneering Inc., San Diego, CA) at 28ºC on a
158 14hr light/10hr dark cycle. All animal work was performed at York University's zebrafish
159 vivarium and in an S2 biosafety laboratory following the Canadian Council for Animal Care
160 guidelines after approval of the study protocol by the York University Animal Care Committee
161 (GZ#2019-7-R2). The *Panx1a* knockout line (*panx1a*$^{-/-}$) was generated and characterized in-
162 house [1-3].

163

164 **Zebrafish Locomotion Assays**. The Zebrabox behavior system and the ZebraLab analytical suite
165 (ViewPoint Life Technology, Lyon, France, http://www.viewpoint.fr) were used for automated
166 extraction of behavioral outputs and video tracking. Tracking videos were recorded at 30 frames
167 per second (fps) under infrared (for Light-OFF recording) or visible light (Light-ON)
168 illumination using a Point Grey Research Dragonfly2 DR2-HIBW camera (Teledyne-FLIR,
169 Burlington, ON, Canada). Inside the Zebrabox a lightbox provided visible and infrared light from
170 below for recordings up to 40% light intensity (visible range, 0-1200 lux). 6dpf larvae were
171 observed in clear 48-well plates maintained at 28ºC throughout the experiment. All experiments
172 were performed between 12:00 to 2 pm, as larvae (6 dpf) activity was previously reported to
173 reach a stable level by early afternoon [4]. Locomotor activity scores (total distance ± SEM.; n = 16
174 per group) were determined from larvae's movements in the time window from 2100 to 2300
175 seconds. Panx1a$^{+/+}$ and Panx1a$^{-/-}$ larvae were exposed to MPTP (Sigma-Aldrich) for four hours
176 prior to recording. The Zebrabox provided a Light-OFF stimulus for 20 minutes at 0% intensity
177 (0 lux), followed by incremental 10% light intensity increases every 10 minutes up to 40% (1200
178 lux). A principal component analysis (PCA) was performed as described [1,5]. The statistical
179 analysis of locomotion data used a Welch's t-test.
180
181 ***In vivo* electrophysiology.** Published procedures were used to prepare anaesthetized 6 days post
182 fertilization (6dpf) zebrafish larvae for *in vivo* electrophysiology [1,6]. Zebrafish larvae at 6dpf were
183 anesthetized using 0.3mM Pancuronium bromide (Sigma-Aldrich, Oakville, ON, Canada) for 2-3
184 min until the touch response stopped. Anesthetized larvae were immobilized in freshly prepared
185 2% low melting temperature agarose. A Leica S9E dissecting microscope (Leica Microsystems,
186 Richmond Hill, ON, Canada) was used to orient the dorsal aspect of the larvae to the gel surface.
187 Embedded larvae were placed on the upright stage of an Olympus BX51 fluorescence microscope

188 (Olympus, Richmond Hill, ON, Canada). Larvae were submerged in 1ml of egg water (E3; pH
189 7.2-7.4) that was applied topically to the agar. Under direct visual guidance two glass
190 microelectrodes (1.2mM OD, approximately 1µM tip diameter, 2-7MΩ), backloaded with 2M
191 NaCl, were placed into the right optic tectum (OT) and the dorsomedial (DM) region of the
192 pallium. Local field potentials were recorded simultaneously from both microelectrodes using a
193 Multiclamp 700B amplifier (Axon Instruments, San Jose, CA, USA). Voltage recordings were
194 low-pass filtered at 1kHz (-3 dB; eight-pole Bessel), high-pass filtered at 0.1 Hz, digitized at 10
195 kHz using a Digidata 1550A A/D interface, and stored on a PC running pClamp11 software (all
196 Axon Instruments). The basal activity was recorded for 10 minutes under Light-ON conditions
197 (1000 lux), during which images of the electrode placement were taken for reference. For each
198 fish, brain activity was normalized to its baseline activity to account for the biological variability
199 of individual brains. In the treatment group larvae were exposed to MPTP (50µM) four hours
200 before recording. A temperature of 28ºC was maintained during experiments.
201
202 **Power spectral density and coherence detection analysis.** A Power spectral density (PSD)
203 estimation was performed by the Welch's method for baseline and MPTP recordings. A moving
204 window for fast Fourier transform (FFT) computation was used and all windows were averaged.
205 The frequency bands theta (3.5-7.5 Hz), beta (12-30 Hz) and gamma (35-45 Hz) were extracted
206 for analysis using NeuroExplorer Version 4 (Nex Technologies, Colorado Springs, CO, 80906,
207 USA). Changes in PSD between baseline and treatment were analyzed for significance using a
208 Welch's t-test. A Coherence analysis was performed applying the Hann method for baseline and
209 MPTP recordings using NeuroExplorer. Changes in the coherence between baseline and
210 treatment were tested for significance using a Welch's t-test.
211

212 **Extracellular ATP Assay.** For quantification of ATP and protein ≈ 50 6dpf larvae were
213 collected at experimental endpoints. Larvae were homogenized in 500µl ice-cold of Phosphate-
214 Buffered Saline (PROBS) containing 100µM ARL-67156 (Sigma-Aldrich) and Halt Protease
215 inhibitor (1:100) (Thermo-Fisher Scientific, Waltham, Massachusetts, USA) for 1min at 30Hz
216 using the Tissuelyser^{LT} (Qiagen, Hilden, Germany). Homogenates were transferred to chilled
217 Eppendorf tubes ($^{-}$20ºC) and centrifuged at 12,000 rpm for 2min. Supernatants were collected and
218 snap-frozen in liquid nitrogen before storage at $^{-}$80ºC. Extracellular ATP measurements used a
219 96-well format (Greiner Bio-One, Monroe, North Carolina, USA) and the Molecular PROBes®
220 ATP determination Kit as described by the manufacturer (Life Technologies, Burlington, ON,
221 Canada). ATP was quantified in replicates of 6 using the Synergy H4 Hybrid Multi-well Plate
222 Reader (Biotek, Winooski, Vermont, USA). The luminescent assay parameters were: plate
223 temperature set to 28ºC; a low-intensity shake of the plate for 3s before reading; a 5s integration
224 time per well; gain setting at 150. In every test, the ATP concentration in experimental samples
225 was calculated from ATP standard curves (0-1µM ATP) included in the same 96-well plate. Data
226 were exported from the Gen5 Data Analysis Software (Biotek) and analyzed in Excel and
227 GraphPad Prism 10. ATP was represented as a normalized concentration per mg of protein. A
228 NanoDrop Spectrophotometer (Thermo Fisher Scientific) was used to measure protein content in
229 2µL of supernatant from homogenized samples. The final ATP content was expressed after
230 normalizing the protein content in each sample of pooled larvae [7]. The data sets were compared
231 using Welch's t-test.
232
233 **Cell Death Assay.** Up to seven larvae (6dpf) were placed into a 2ml Eppendorf tube in egg
234 water. MPTP treatment (20µM) was applied for four hours. During the last 60mins, acridine
235 orange (2.5µl/ml; Sigma-Aldrich) was added to the Eppendorf tube. Following incubation, the

236 larvae freely swam in 10ml fresh egg water for 10 minutes to remove excess AO. Then, the
237 larvae were immobilized using the muscle relaxant pancuronium bromide and mounted head
238 down in 2% agar noble in dishes. Cell death was imaged using a Zeiss LSM700 (Objective 10x
239 NA0.8; Z-stack ≈ 100µm). All parameters were controlled by ZEN software (ZEISS, North York,
240 ON, Canada) and consistently applied. Raw 3D volumes were processed for AO-positive cell
241 detection using Bitplane-Imaris software (Oxford Instruments, Abingdon, UK). Statistics used
242 unpaired t-test and GraphPad Prism 10.
243
244 **NGS RNA-sequencing.** The transcriptomes of all zebrafish lines used in this research were
245 analyzed by RNA-seq (NGS-Facility, The Center for Applied Genomics, SickKids, Toronto, ON,
246 Canada). The reported data was derived from the sequencing of three independent pools of ≈30
247 age-matched larvae (6dpf). The RNA-seq data are deposited at the NCBI - Gene Expression
248 Omnibus (GEO) database repository (ID pending). Total RNAs were extracted from 30 6dpf
249 larvae using RNeasy Plus Mini Kit (Qiagen). The RNA quality was determined using a
250 Bioanalyzer 2100 DNA High Sensitivity chip (Agilent Technologies, Mississauga, ON, Canada).
251 The RNA library preparation was performed following the NEB NEBNext Ultra II Directional
252 RNA Library Preparation protocol (New England Biolabs Inc., Ipswich, MA, USA). RNA
253 libraries were loaded on a Bioanalyzer 2100 DNA High Sensitivity chip to check for size,
254 quantified by qPCR using the Kapa Library Quantification Illumina/ABI Prism Kit protocol
255 (KAPA Biosystems, Wilmington, MA, USA). Pooled libraries were paired-end sequenced on a
256 High Throughput Run Mode flow cell with the V4 sequencing chemistry on an Illumina HiSeq
257 2500 platform (Illumina, Inc., San Diego, CA) following Illumina's recommended protocol to
258 generate paired-end reads of 126-bases in length.
259

260 **Differential Gene Expression and Functional Enrichment Analyses.** The post-sequencing
261 processing to final read counts, normalization, and differential gene expression analysis used
262 multiple software packages, including a two-condition differential expression analysis using the
263 edgeR R-package, v.3.8.6 [8,9] and DESeq2 R package version 1.40.2 [10]. Genotypes and treatments
264 were incorporated into the statistical model and multiple hypothesis testing was performed. The
265 default filter for DESeq2 used a threshold of $p<0.05$ and the Benjamini-Hochberg procedure to
266 determine the false discovery rate (FDR), and the adjusted P-value (padj). Differential gene
267 expression was defined as log2FoldChange >2 or <-2, respectively.

268 A Gene Set Enrichment Analysis (GSEA) tested whether a defined set of genes shows
269 statistically significant, concordant differences between genotypes and treatment groups. This
270 method calculates sample-wise gene set enrichment scores and estimates variation of pathway
271 activity over a sample population in an unsupervised manner [10]. The Molecular Signatures
272 Database (MSigDB) v.5.2 (http://software.broadinstitute.org/gsea/msigdb/index.jsp), a renowned
273 repository of curated gene sets encompassing diverse biological pathways was used to source
274 gene sets for broad Hallmarks. Before GSEA RNA-seq data were filtered at padj < 0.01 to
275 increase the stringency of the analysis. Other tools used to process RNA-seq data were HCOP
276 (https://www.genenames.org/tools/hcop/) and db2db at bioDBnet
277 (https://biodbnet.abcc.ncifcrf.gov/db/db2db.php) to convert curated human or mouse to zebrafish
278 genes [11,12]. Curated gene lists were generate with information from the Zebrafish Information
279 Network (ZFIN) (https://zfin.org/) and the KEGG (Kyoto Encyclopedia of Genes and Genomes,
280 https://www.genome.jp/kegg/) databases, and using unique qualifiers from the Gene Ontology
281 (GO) project (https://geneontology.org/).
282

283 **Pharmacology**. All chemicals were purchased from Sigma-Aldrich (Mississauga, Canada):
284 (MPTP; 1-50µM; cat#: M0896), Pancuronium bromide (Panc; 300µM; cat#P1918), Acridine-
285 Orange (AO; 15µM; cat#: A6014). All reagents were water-soluble. The concentrations referred
286 to in results are final.
287
288 **Statistics and data reproducibility. S**tatistical analyses were performed in NeuroExplorer VS4,
289 or in GraphPad Prism VS10. Results are represented as the mean ± standard error of the mean
290 (SEM). For molecular analysis (RNA-seq, ATP detection), a minimum of $n \geq 3$ independent
291 experimental replicates were generated. For behavioral testing G*power analysis determined the
292 number of larvae [1,5]. The normality and homogeneity of the data variance were determined by the
293 "Shapiro-Wilk Test" and "Levene's Test." Experimental groups were compared using unpaired t-
294 tests or Welch's t-tests. A P value <0.05 was considered statistically significant. For all
295 experiments, sample sizes, statistical tests, and when appropriate P values are indicated in the
296 figure legends.
297
298 **Results**
299 ***Acute MPTP treatment the locomotion of zebrafish larvae.***
300 Acute MPTP treatment for four hours was evaluated to establish a practical alternative of
301 targeting mitochondrial metabolism in dopaminergic neurons during a critical developmental
302 stage. The six-days post fertilization (6dpf) timepoint was chosen based on the expression profile
303 of Panx1 genes in rodents and fish; the expression reaches a transient peak before birth in rodents
304 [13], and when zebrafish transition to free-swimming juveniles.
305 To assess the impact of MPTP treatment, we utilized a modified visual-motor response
306 (VMR) assay, measuring zebrafish larvae responsiveness to gradual Light-ON changes up to

307 1200 lux after a period of Light-Off **(Fig 1a).** A principal component analysis (PCA) of 11
308 swimming behavioral parameters, captured over 72% (PC1) and 24% (PC2) of the data variance,
309 respectively**.** The total swim distance (PC1, *totaldist*) was used to quantify differences between
310 MPTP-treated and untreated genotypes **(Fig. 1b)**.

311 In the VMR assay, both Panx1a$^{+/+}$ and Panx1a$^{-/-}$ larvae responded to MPTP treatment
312 (1µM to 50µM) in Light-ON conditions, with a decline in swimming distance as the MPTP dose
313 increased **(Fig. 1c).** Acute MPTP treatment consistently decreased swimming activity in both
314 Panx1a$^{+/+MPTP}$ and Panx1a$^{-/-MPTP}$ larvae compared to untreated controls, even at the lowest
315 concentration tested. The average total distance covered in a 10-second time bin was 25.6 $\pm$ 0.8
316 mm (Panx1a$^{+/+}$) and 21.1 $\pm$ 0.4 mm (Panx1a$^{-/-}$), with no statistically significant differences
317 between genotypes in the presence of MPTP. **Fig. 1d** shows that the initial Light-OFF period
318 reduced swimming distance to a baseline, followed by the resumption of swimming activity in
319 untreated larvae as light increased from 10% (400 lux) to 40% (1200 lux) Light-ON over the next
320 40 minutes. This result underscores the impact of Panx1a ablation and acute MPTP treatment on
321 the visuomotor response in 6dpf zebrafish larvae.
322

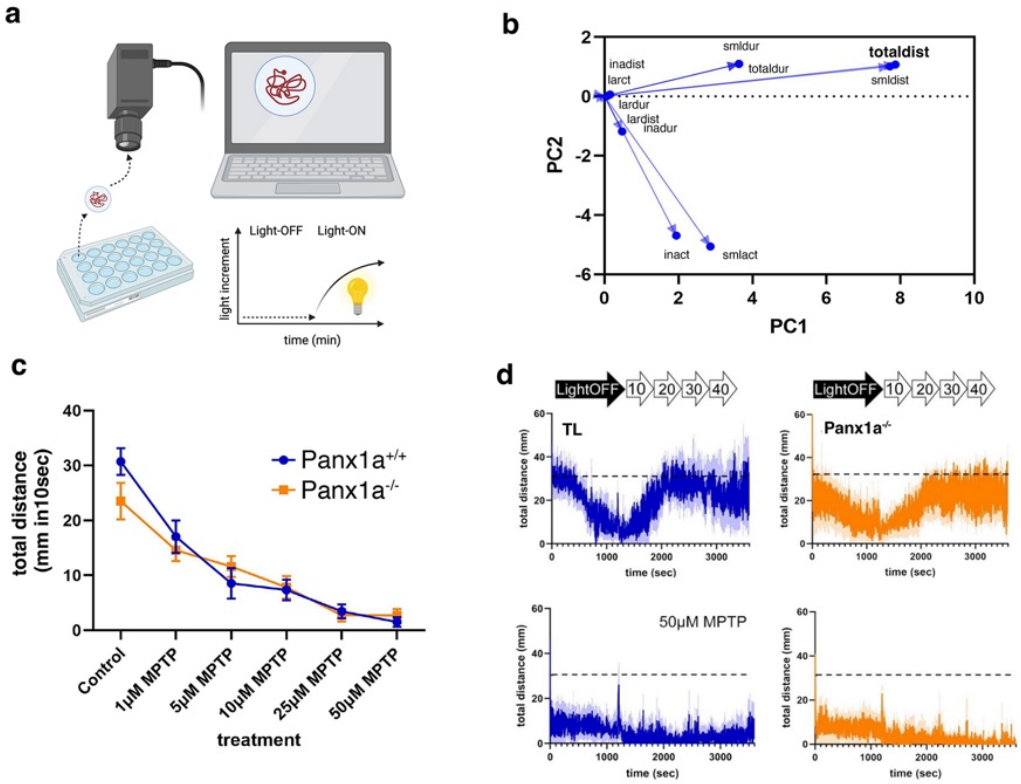

Figure 1: ***Acute MPTP treatment alters zebrafish locomotion.*** a) Experimental setup for video recording and light stimulation of 6dpf larvae during a modified visual-motor response (VMR) assay. b) Principal Component Analysis of 11 behavioral parameters. c) Concentration-dependent impact of acute MPTP treatment on swimming behavior without (control) or after 4hrs exposure. d) Cumulative traces representing the Mean (dark blue/orange) and SEM (light blue/orange) for n=16 larvae/genotype and MPTP treatment condition. The horizontal dashed line indicates the average total swimming distance of untreated Panx1a$^{+/+}$ larvae. Statistics: Student t-test; Values represent Mean ± SEM for total distance of swimming in mm in a 10-second time-bin. The image in a) was created with BioRender.

Panx1a$^{+/+MPTP}$ and Panx1a$^{-/-MPTP}$ larvae show different transcriptional responses associated with altered mitochondrial metabolism, cell homeostasis, and cell death.

To gain insight into the molecular basis of the observed behavioral changes experimental RNA-seq analysis and a computational approach compared MPTP-treated Panx1a knockout (Panx1a$^{-/-MPTP}$) and wild-type (Panx1a$^{+/+MPTP}$) larvae with naïve siblings, unraveling key regulatory pathways underlying MPTP neurotoxicity in the model. Gene expression profiles of

340 Panx1a$^{-/-}$ and Panx1a$^{+/+}$ larvae were different before MPTP exposure; RNA-seq identified a total
341 of 31251 individual RNA transcripts, with n=724 genes upregulated and n=1030 genes
342 downregulated in the knockout group compared to wild-type controls **(Fig.2a)**. Following the
343 exposure to MPTP (4 hours), both genotypes exhibited substantial alterations in gene expression
344 patterns, highlighting the dynamic nature of the cellular response to MPTP. Notably, the
345 magnitude of gene expression dysregulation was markedly amplified in Panx1a$^{-/-MPTP}$ larvae post-
346 treatment compared to Panx1a$^{+/+MPTP}$ counterparts (downregulated: Panx1a$^{+/+MPTP}$ n=3764 genes,
347 Panx1a$^{-/-MPTP}$ n=4828 genes; upregulated: Panx1a-$^{+/+MPTP}$ n=3500 genes, Panx1a$^{-/-MPTP}$ n=4749
348 genes; false discovery rate: FDR < 0.05) **(Fig. 2b,c)**.

349 To interpret the biological pathways perturbed by MPTP treatment, we conducted a gene
350 set enrichment analysis (GSEA) [14]. The visualization of enrichment within the top 50 Hallmarks
351 pathways provided first insights into intricate regulatory networks modulating neuronal responses
352 to MPTP exposure in the context of Panx1a ablation. Our analysis revealed significant
353 enrichment of pathways associated with metabolism and cell death, including oxidative
354 phosphorylation (Oxiphospho), glycolysis, reactive oxygen species (ROS) regulation,
355 mammalian target of rapamycin complex 1 (mTORC1) signaling, fatty acid metabolism, and
356 hypoxia. Considering the mitochondrial dysfunction in MPTP-induced neurotoxicity, the next
357 step of our investigation prioritized the analysis of how Panx1a ablation affected pathways linked
358 to mitochondrial homeostasis.

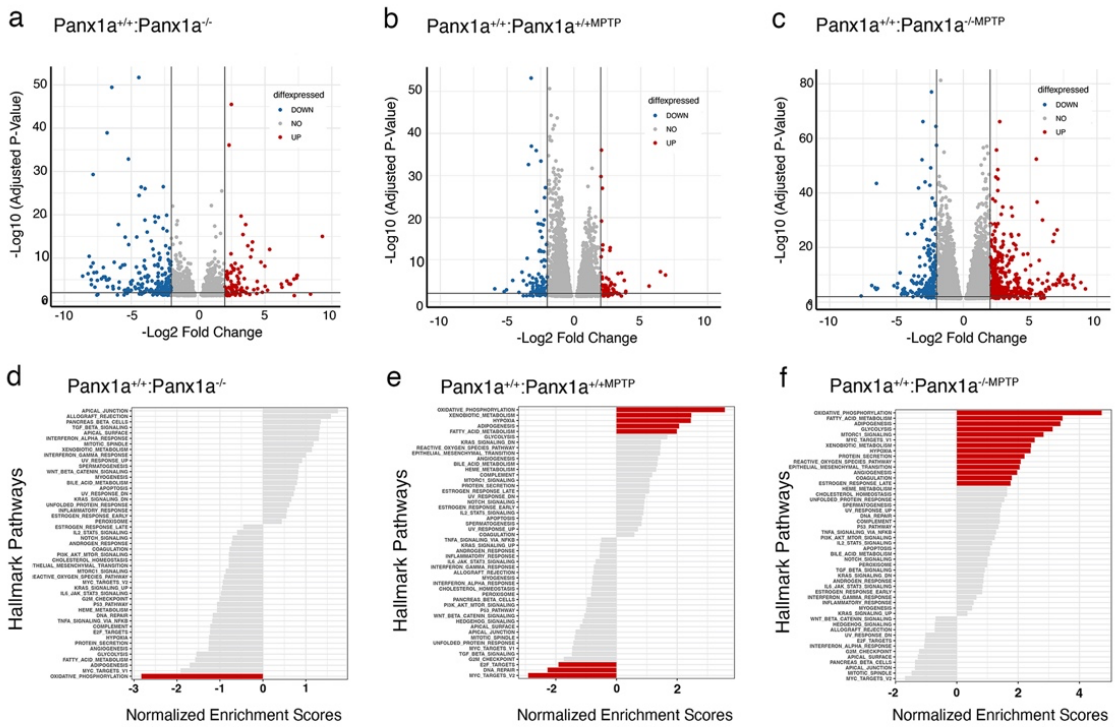

Figure 2: *MPTP treatment caused greater disruption of gene expression in Panx1a$^{-/-}$ larvae*. a-c) illustrates the log2 fold change of differentially expressed genes pre- and post-MPTP exposure, with changes exceeding a two-fold threshold highlighted in red (upregulated) or blue (downregulated). d-f) Gene set enrichment analysis (GSEA) revealing normalized enrichment scores (NES) for the top 50 ranked Hallmark pathways. Enriched pathways are denoted in red (threshold: padj <0.05), indicating noteworthy alterations in biological processes associated with MPTP treatment in knock-out larvae compared to wild-type counterparts.

The MPTP-induced metabolic crisis altered pathways regulating hypoxia, reactive oxygen species, and fatty acid homeostasis.

A comprehensive computational analysis, leveraging GSEA, explored the impact of MPTP treatment on Panx1a$^{+/+}$ and Panx1a$^{-/-}$ zebrafish larvae's mitochondrial health. The GSEA result demonstrated an enrichment of the oxidative phosphorylation pathway in both Panx1a$^{+/+MPTP}$ (n=100) and Panx1a$^{-/-MPTP}$ larvae (n=155) with a log2 fold filter set to >0.5 and <-

375 0.5 and a padj of <0.01 **(Fig. 3a)**. Only n=38 genes were different in untreated controls showing
376 that MPTP treatment impacted this pathway significantly.

377 The notable differential gene expression modulation and directionality of changes in
378 Panx1a$^{-/-MPTP}$ larvae was also found in biological processes downstream of oxidative
379 phosphorylation, such as *GO:0006096 – Glycolysis*, *GO:0001666 - Response to Hypoxia*,
380 *GO:0000302 - Response to reactive oxygen species (ROS), GO:0030968 - Unfolded Protein*
381 *Response (UPR), and GO:0006631 - Fatty acid metabolic process* **(Fig. 3d-h; Suppl. Tables 2-**
382 **6)**.

383 Notable Panx1a$^{-/-MPTP}$ specific regulations of glycolysis genes were the dysregulation of
384 two enolase genes, *eno1a/b* and *eno2*, key enzymes for cellular bioenergetics, without which
385 glycolysis cannot produce ATP, which reduces hypoxia tolerance **(Fig. 3d, Suppl. Table 2)**.
386 Likewise, the differential expression of pyruvate kinases *pkma/b*, phosphofructokinases *pfkma/b*,
387 and phosphoglycerate mutase A (*pgam1a*) demonstrate the switch to an oxygen-independent, and
388 relatively inefficient way of ATP generation when Complex I is blocked by MPTP treatment.

389 Furthermore, MPTP treatment caused the differential expression of hypoxia or ROS
390 related pathways in Panx1a$^{-/-MPTP}$ larvae that can promote neuronal cell death (*hif1al, ldha, ddit4,*
391 *egln3*) **(Fig. 3 e,f, Suppl. Tables 3,4)**. A notable change to expression in the unfolded protein
392 response (UPR) was a gene encoding for a protein, *sec13*, that functions as an activator of the
393 amino acid-sensing branch of the mTORC1 signaling pathway **(Fig. 3g; Suppl. Table 5)**. Other
394 regulated genes like *fktn, chac1, atf4a* are part of a signaling complex linked to synaptic function.
395 More specifically, the mammalian homolog of *fktn* regulates synaptic function via inhibition of
396 the ATF4 transcription factors complex with DISC1 (Disrupted-in-schizophrenia 1), or function
397 like *chac1*as a pro-apoptotic component of the unfolded protein response pathway by mediating
398 the pro-apoptotic effects of the ATF4 in the ATF4-ATF3-DDIT3/CHOP cascade.

399 The notable upregulation of *Fatty acid metabolic process* (GO:0006631) illustrated how
400 Panx1a ablation affected energy homeostasis **(Fig. 3h; Suppl. Table 6)**. For example, the
401 upregulated fatty acid elongation enzymes represented by *elovl1b, elovl4b, elovl5,* or *elovl7a/b*
402 are important for the mitochondrial fatty acid β-oxidation, the major pathway for the degradation
403 of fatty acids that is essential for maintaining energy homeostasis. The transcriptional regulation
404 of five apolipoproteins *apoea/b, apoa1a, apobb.1*, and *apoc1* signified pleiotropic effects on
405 lipoprotein metabolism. The upregulation of *apoea/b* was notable since human ortholog(s) are
406 implicated in multiple diseases, including Alzheimer's disease, artery disease, cerebrovascular
407 disease, eye disease, and familial hyperlipidemia. We reasoned that an accumulation of fatty
408 acids in mitochondria above physiological levels could have harmed mitochondrial function in
409 Panx1a$^{-/-MPTP}$ larvae causing the observed changes to hypoxia and reactive oxygen species-related
410 processes.

411 We hypothesized that the altered expression of genes in the oxidative phosphorylation
412 pathway affected ATP production, with the absence of the ATP-release channel Panx1a
413 amplifying the effect of Complex I blockage by MPP+. To validate this hypothesis, we quantified
414 extracellular ATP concentrations both before and after MPTP treatment in both genotypes. The
415 impact of MPTP treatment on extracellular ATP levels was pronounced in Panx1a$^{+/+MPTP}$ larvae,
416 demonstrating a significant reduction (Panx1a$^{+/+}$: 3.12 $\pm$ 0.28 nM/µg; Panx1a$^{+/+MPTP}$: 0.96 $\pm$ 0.27
417 nM/µg; P-value=0.0011), indicating a limitation in ATP production **(Fig. 3i)**. Conversely, MPTP
418 treatment had a minor effect on Panx1a$^{-/-MPTP}$ larvae, revealing a decrease of low ATP levels
419 (Panx1a$^{-/-}$: 1.73 $\pm$ 0.31 nM/µg; Panx1a$^{-/-MPTP}$: 0.95 $\pm$ 0.15 nM/µg; P-value=0.044).

420 The upregulation of mitochondrial Complex I and Complex III genes, NADH:ubiquinone
421 oxidoreductase subunit A11 (*ndufa11*), or ubiquinol-cytochrome c oxidoreductases (*uqcr10,*
422 *uqcrfs1*), illustrate changes to mitochondrial energy metabolism and homeostasis which are

amplified in Panx1a$^{-/-MPTP}$ larvae. The augmented upregulation of pathways leading to hypoxia, ROS-production, or the unfolded protein response further substantiate that Panx1a is required to maintain metabolic and energetic homeostasis *in vivo*.

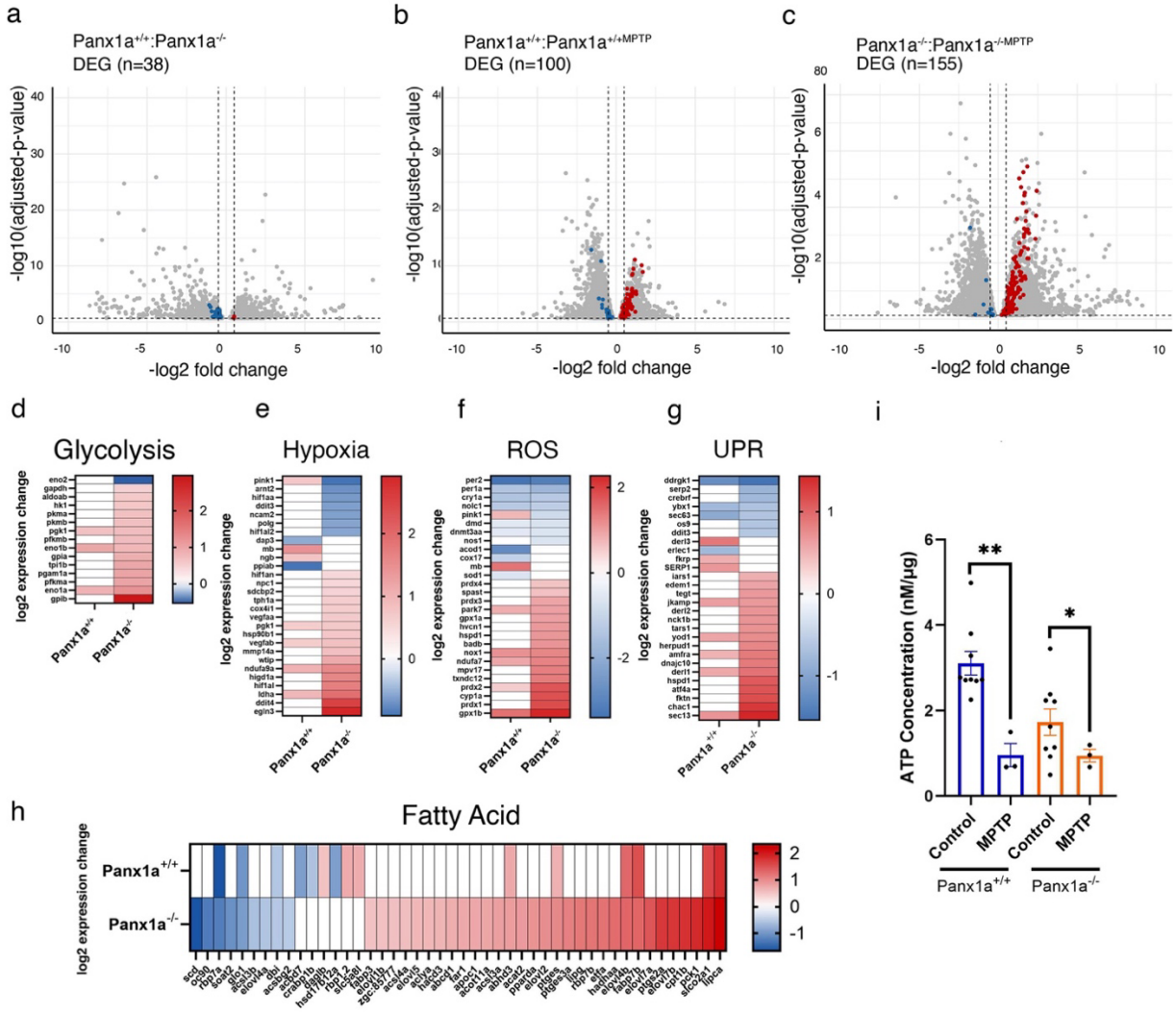

Figure 3: *Acute treatment with MPTP caused a metabolic crisis and reduced ATP release in Panx1a$^{+/+}$ larvae*. a-c) Differentially expressed genes in the oxidative phosphorylation pathway. Dots in blue and red represent significantly regulated genes in the oxidative phosphorylation pathway. Grey dots represent all DEGs. d-h) Heatmaps illustrate the differential expression of genes identified in the biological processes: GO:0006096 – *Glycolysis*, GO:0001666 - *Response to Hypoxia*, GO:0000302 - *Response to reactive oxygen species* (ROS), GO:0030968 - *Unfolded Protein Response (UPR)*, and GO:0006631 - *Fatty acid metabolic process*. i) ATP concentrations were measured before and after acute MPTP treatment. MPTP treatment caused a significant downregulation in Panx1a$^{+/+MPTP}$ larvae (P-value < 0.05). No significant differences in ATP

437 concentrations were observed in Panx1a$^{-/-MPTP}$ larvae. The ATP concentrations were adjusted for
438 protein concentration to evaluate extracellular ATP levels across multiple samples. Each sample
439 represented a pool of 50 6dpf larvae. Statistical approach: Welch's t-test. The number of
440 experimental replicates: Panx1a$^{+/+}$ and Panx1a$^{-/-}$ untreated controls n=9; MPTP treatment
441 conditions n=3. Mean ± SEM. Statistical significance was indicated as *: P-value * <0.05, ns =
442 not significant.
443

444 ***Loss of Panx1a and activation of oxidative phosphorylation alters the AMPK-mTOR pathway***

445 The enrichment of the mTORC1 hallmark, identified through GSEA (see Fig. 2), implied
446 mechanistically a switch towards anabolic metabolism. The differential gene expression of
447 mTORC1 pathway genes in untreated controls (n=13), Panx1$^{+/+MPTP}$ (n= 74), and Panx1a$^{-/-MPTP}$
448 larvae (n=121) exhibited an enrichment trend that showed that Panx1a$^{-/-MPTP}$ were affected most
449 by the oxidative phosphorylation (OXIPHOS) dysfunction **(Fig. 4a-c)**. The upregulation of the
450 AMP-activated protein kinase (*prkaa1*/AMPK), a master regulator of cellular energy
451 homeostasis, together with genes in the AMPK pathway in Panx1a$^{-/-MPTP}$ larvae further suggested
452 that a molecular response to stresses that deplete cellular ATP supplies such as Complex I
453 blockage was found **(Fig. 4a-c)**.

454 To identify specific molecular pathways in response to stress when cellular ATP is
455 depleted in Panx1a$^{-/-MPTP}$ larvae we used STRING analysis to infer context **(Fig. 4d)**. The input
456 were 54 AMPK-mTOR pathway genes, ranked by their log2fold expression. K-means clustering
457 identified five clusters specific for Panx1a$^{-/-MPTP}$ larvae. Notable groups of genes upregulated in
458 the mTOR pathway included nine Wnt/frizzled genes in Cluster I (*wnt5a, wnt7aa, wnt9a/b,*
459 *wnt10a, wnt11, fdz6, fdz7a/b*). Activation of the canonical Wnt-signaling pathway in neurons
460 could enhance both hexose utilization through glycolysis and regulate dendrite formation and
461 complexity. Indeed, Cluster II encompasses 16 genes representing fructose and mannose
462 metabolism. Cluster II linked to Cluster III through upregulated *prkaa1a/AMPK* and *pik3r3a.* The
463 1-phosphatidylinositol-3-kinase regulator activity acts upstream of the insulin receptor signaling

464 pathway and the phosphatidylinositol phosphate biosynthetic process. Within Cluster III the
465 upregulation of four subunits of vacuolar ATPases (*V-ATPase; atp6v1aa atp6v1ab atp6v1b2,*
466 *atp6v1g1 atp6v1h atp6v1c1b atp6v1ba atp6v1f*) implicated a disruption of presynaptic cellular
467 homeostasis in neurons. Furthermore, late endosomal/lysosomal adaptor and MAPK and mTOR
468 activator genes (*lamtor5*) and Ras-related GTP-binding protein A (*rraga*) encode proteins
469 forming the Lamtor/Ragulator complex that regulates multiprotein signaling units on late
470 endosomes/lysosomes with crucial roles in the cellular response to amino acid availability
471 through regulation of the mTORC1 signaling cascade.

472 The downregulation of RAF activation (Cluster IV) indicated the complexity of molecular
473 pathway changes affected by Panx1a ablation in cell stress. A reduction of RAF activation as an
474 entry point to the mitogen-activated protein kinase (MAPK)/extracellular signal-regulated kinase
475 (ERK-1/2) signaling pathway, suggested effects on fundamental cellular functions including
476 proliferation, differentiation, and survival.

477 The adiponectin signaling pathway, and the Adiponectin activated signaling pathway
478 (Cluster 5) involved two receptors that are required for normal glucose and fat homeostasis. In
479 mice AdipoR1 and AdipoR2 are present in the synaptosome, with AdipoR2 displaying increased
480 presynaptic vs. postsynaptic localization, whereas AdipoR1 was enriched in both the presynaptic
481 and postsynaptic fractions. Loss of function mutations in mouse KO models support transsynaptic
482 roles causing cognitive deficits.

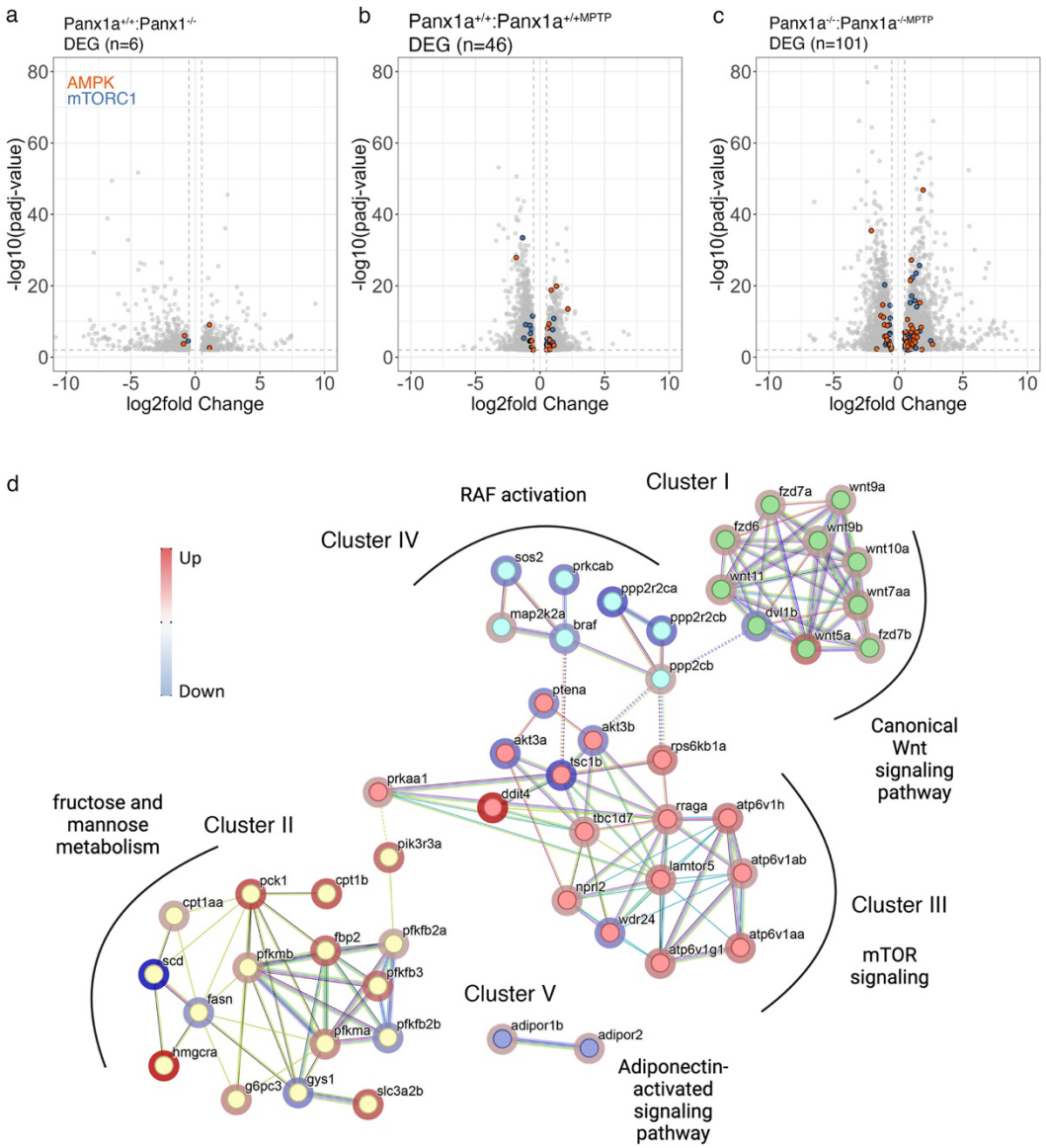

483

484 **Figure 4:** *Loss of Panx1a and activation of oxidative phosphorylation alters the AMPK-mTOR*
485 *pathway.* a- c) Vulcano plots represent the differential expression of AMPK- (orange) and
486 mTORC1 (blue) pathway genes. d) STRING analysis of 49 genes. K-means clustering identified
487 five clustered groups.
488

489

490 ***Loss of Panx1a and activation of oxidative phosphorylation promotes cell death pathways.***

491 The enrichment of the mTORC1 pathway observed in the GSEA analysis suggested
492 responses to metabolic and other stresses. A follow-up of the differential expression regulation of
493 192 mTOR pathway genes identified 121 regulated genes in Panx1a$^{-/-MPTP}$ larvae. Fewer genes
494 were differentially regulated in Panx1a$^{+/+}$ (n=14) and Panx1a$^{+/+MPTP\ larvae}$ (n=74) **(Fig. 5a)**.

495 The upregulation of eight subunits of vacuolar ATPases (*V-ATPase; atp6v1aa atp6v1ab*
496 *atp6v1b2, atp6v1g1 atp6v1h atp6v1c1b atp6v1ba atp6v1f*) and late endosomal/lysosomal adaptor
497 and MAPK and mTOR activator genes (LAMTOR/Ragulator) encoding scaffold proteins
498 forming complexes that regulate multiprotein signaling units on late endosomes/lysosomes were
499 involved in acidification (*lamtor2, lamtor3, lamtor5*). We propose that the upregulation of these
500 components could reflect an attempt by the cell to adapt to stress by enhancing lysosomal
501 function and autophagy.

502 These changes suggested that systems in MPTP-related larvae in the absence of Panx1a
503 were overwhelmed or dysfunctional due to an inability to maintain cellular homeostasis, leading
504 to cell death. The functional enrichment analysis showed differentially expressed genes
505 associated with cell death (GO:0008219), autophagy (GO:0006914), and the execution phase of
506 apoptosis (GO:0097194). In Panx1a$^{-/-MPTP}$ larvae, 223 cell death-related genes were identified,
507 while Panx1a$^{+/+MPTP}$ larvae exhibited regulation in 107 genes **(Fig 5b, Suppl Table 7)**. The
508 analysis of autophagy genes mirrored the overall pattern of cell death, with a substantial six to
509 eleven-fold increase in differentially expressed genes when comparing untreated with MPTP-
510 treated larvae (Panx1a$^{+/+MPTP}$, n=38; Panx1a$^{-/-MPTP}$, n=70) **(Fig. 5c)**. The unique molecular
511 response in the absence of Panx1a was evident, with Panx1a$^{-/-MPTP}$ larvae showing a notable
512 increase in differentially upregulated (n=35) and downregulated genes (n=16) **(Suppl Table 8)**.
513 Among the upregulated genes, transmembrane 41b (*tmem41b*), tumor protein p53-inducible

514 nuclear protein 1 (*tp53inp1*), and the stimulator of interferon (*sting1*), pointed towards the
515 activation of autophagy and cellular stress response. These genes play essential roles in
516 autophagosome biogenesis, pro-apoptotic responses, and inflammation mediation, respectively,
517 contributing to cellular adaptations and responses under MPTP-induced conditions.

518 Activation of the execution phase of apoptosis was observed in Panx1a$^{-/-MPTP}$ larvae, as
519 demonstrated by the upregulation of seven members of the caspase gene family, including
520 initiators of apoptosis *casp9* and *casp20*, and executioner phase caspases *casp3a, casp6a,*
521 *casp6b1*, and *casp7*. The log2 fold ratio = 7.15 upregulation of the inflammatory caspase *caspbl*
522 (alternative name casp19b) was particularly notable as a hallmark for the execution phase of
523 apoptosis, downstream of the assembly of the inflammasome complex, leading to the cleavage
524 and activation of the proinflammatory cytokine *il1b* **(Fig. 5f, Suppl Table 9)**.

525 An *in-vivo* cell death stain, acridine orange (AO), was chosen as a direct way of
526 visualizing cell death **(Fig. 5g).** Notably, AO-stained nuclei were particularly prominent in brain
527 regions known for dopaminergic neuron expression or the optic tectum, which receives inputs
528 from hypothalamic dopaminergic neurons. In the absence of treatment, Panx1a$^{+/+}$ larvae exhibited
529 the lowest number of dead cells (Panx1a$^{+/+}$ = 39.67, Panx1a$^{-/-}$ = 66). The number of AO-positive
530 cells in Panx1a$^{-/-}$ larvae was significantly higher compared to Panx1a$^{+/+}$ (P-value = 0.0056) **(Fig.**
531 **5h)**. MPTP treatment increased cell death in both genotypes (P-value = 0.0130), with an average
532 of n=174 AO-positive cells in Panx1a$^{-/-MPTP}$ and n=125 in Panx1a$^{+/+MPTP}$ larvae.

533 In summary, the results underscore a multifaceted role for Panx1a in modulating gene
534 expression related to cell death, apoptosis, and autophagy. Imaging of cell death *in vivo*
535 implicates regions with loss of dopaminergic neurons.

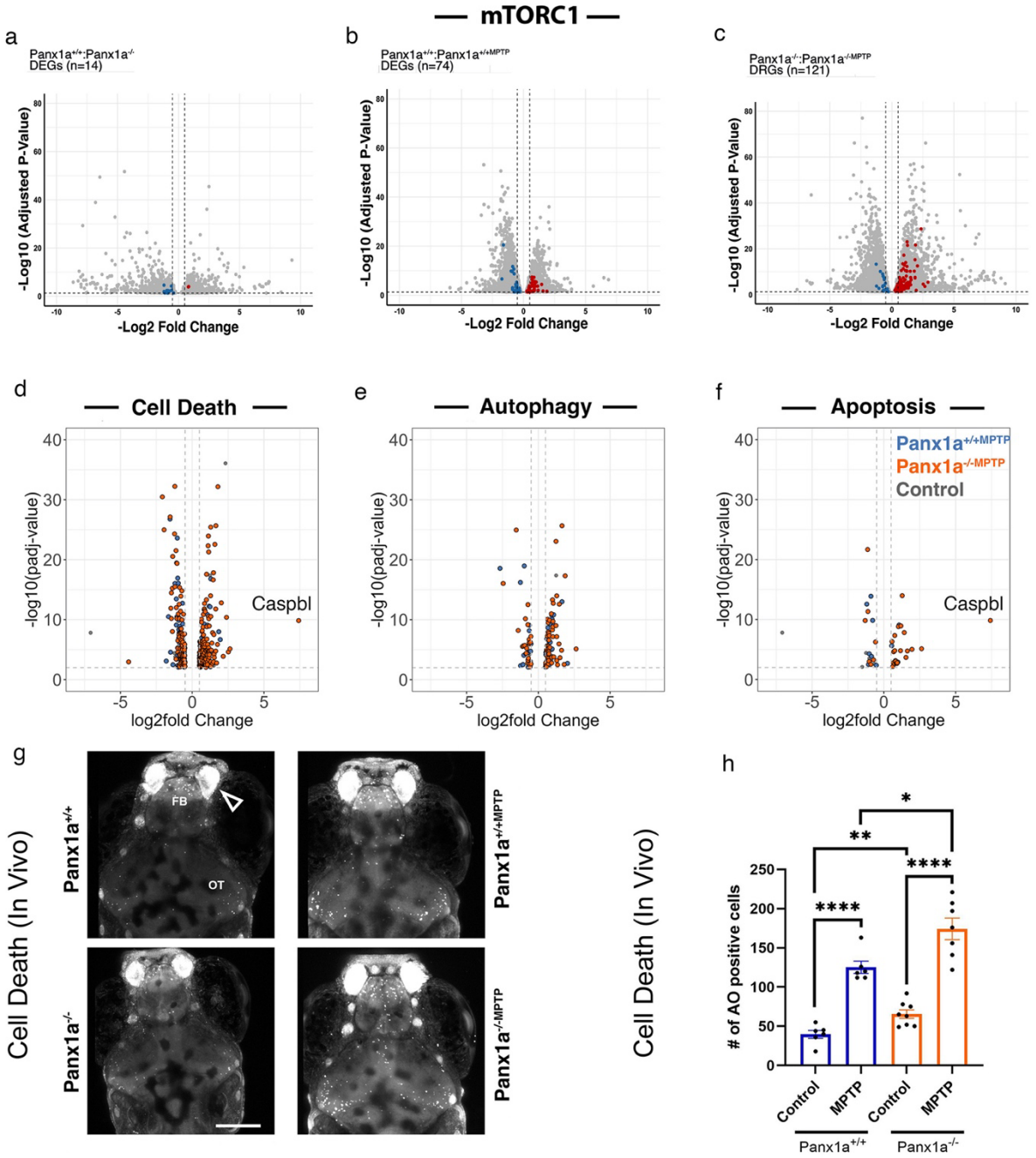

Figure 5: *Loss of Panx1a promotes cell death in the acute MPTP model.* a-c) Differentially regulated genes in the mTORC1 pathway. Blue and red dots represent regulated genes in the pathway. Grey dots represent all DEGs. d-f) Significantly regulated genes (padj ≤ 0.01) were compared against zfin lists of cell death, apoptosis, and autophagy. Regulated genes were plotted. g) Experimental outline of the *in-vivo* cell death assay using the acridine orange dye. Representative projection views of Z-stacks representing a depth ≈ 100µm collected from untreated and MPTP-treated Panx1a$^{+/+}$ and Panx1a$^{-/-}$ larvae. h) Quantification of acridine-orange positive cells. Statistical approach: Significance was calculated using an unpaired t-test. Number

546 of larvae, n=7 for all treatments. Mean ± SEM. Statistical significance was indicated as *: P-
547 values * <0.05, ** <0.01, *** <0.005, **** <0.001.
548

549

550 ***Trans-synaptic changes after Panx1a ablation and MPTP treatment***

551 A DESeq2 analysis of the RNA sequencing analysis, employing a log2 gene filter of >0.5
552 and <-0.5 with a padj < 0.01, identified 681 differentially expressed genes in Panx1$^{-/-MPTP}$ and
553 Panx1$^{+/+MPTP}$ larvae. The analysis of the Gene Ontology search terms *GO:Biological Process* and
554 *GO:Cellular Compartment* indicated significant upregulation of biosynthetic pathways,
555 suggestive of increased metabolic activities in 6dpf larvae with Panx1a ablation **(Fig. 6a,b)**.
556 Conversely, downregulated genes were enriched for biological processes related to
557 neurotransmission at chemical synapses, synaptic signaling, and neurodevelopment, affecting
558 both pre- and postsynaptic compartments. Specifically, the query term *GO:0045202 – Synapse*
559 identified 53 downregulated genes and no upregulated genes, while the terms *GO:0098793 –*
560 *Presynapse* and *GO:0098794 – Postsynapse* identified 35 and 36 differentially expressed genes,
561 respectively **(Fig. 6c,d; Suppl Table 10)**.

562 STRING analysis of the downregulated genes demonstrated a significant impact of
563 Panx1a ablation on GABAergic and glutamatergic transmission. Notably, ligand-gated and G
564 protein-coupled GABA receptor subtypes *(gabra6b, gabrb1, gabrb3, gabrb4, gabrz, gabrg2,*
565 *gabrr2a)* (**Cluster I)**, ionotropic NMDA (*grin2aa, grin2ab, grin2bb*), AMPA (*gria4a*), and
566 kainite receptors (*grik2*) were downregulated alongside other regulators of synaptic plasticity
567 (**Cluster II Suppl. Fig. 1**). For example, the mouse ortholog of *shisa9a* is known as a regulator
568 of short-term neuronal synaptic plasticity in the dentate gyrus associated with AMPA receptor
569 function. Likewise, the discs large MAGUK scaffold protein genes *dlg2* (PSD93) and *dlg4*
570 (PSD95) were downregulated.

571 **Cluster III** encompassed genes encoding pre-synaptic proteins with essential roles in
572 neurotransmitter release via the formation of the soluble N-ethylmaleimide-sensitive fusion
573 protein attachment protein receptors (SNARE) complex (synaptosomal-associated protein:
574 *snap25a, snap25b*), vesicle exocytosis or calcium dynamics in response to depolarization
575 (synaptotagmin: *syt1a, syt5b*; syntaxin: *stx1b, stx12l, stxbp1a*; complexin; *cplx2, cplx2l, cplx3b,*
576 *cplx4a*). The presynaptic downregulation of glutamate decarboxylase gene 2 (*gad2*) expression is
577 notable; the Gad2 protein catalyzes the presynaptic production of GABA, which suggests a
578 negative feedback loop as downregulation of GABA production corresponds with reduced
579 GABA receptor expression.

580 Furthermore, deregulation of inorganic ion transporters (n=45) and calcium binding
581 proteins (n=27) was observed in Panx1a$^{-/-MPTP}$ larvae **(Fig. 6d).** Synaptically localized anionic ion
582 transporters (n=15) with reduced expression in the nervous system **(Suppl. Fig 1, Clusters I, II)**
583 included AMPA and NMDA receptors, or chloride permeable GABA receptors. The four up-
584 regulated genes included a Na-Cl cotransporter-like protein (*slc12a10.2*), an anion:anion
585 antiporter with bicarbonate transmembrane transporter activity (*slc4a1b*), or a gene encoding a
586 voltage-gated chloride channel (*clcn2c*) that maintains chloride ion homeostasis. Deregulation of
587 cation transporters (n=25) included transporters and channels permeable for potassium (*kcna1b,*
588 *kcnip1b, kcnip3b, kcn1a.1, kcnk3b*), calcium (*cacna1fb, cacna1ha*), sodium (*scn3b*), or co-
589 transporters for sodium and chloride (*slc12a10.2*), symporters for potassium and chloride
590 (*slc12a5b*), a potassium-dependent sodium/calcium exchanger (*slc24a5*), or a
591 GABA:sodium:chloride symporter (*slc6a1a*). The loss of Panx1a also affected the differential
592 expression of calcium-binding proteins (n=26). Notable examples include members of the
593 protocadherin gene family (*pcdh1a, pcdh8, pcdh17, pcdh19*) regulating neurotransmission and
594 synaptic plasticity.

Overall, the computational analysis suggested that Panx1a ablation, in conjunction with MPTP treatment, perturbed ion homeostasis and neurotransmitter release at synapses, affecting neurotransmission and synaptic plasticity across pre- and postsynaptic compartments.

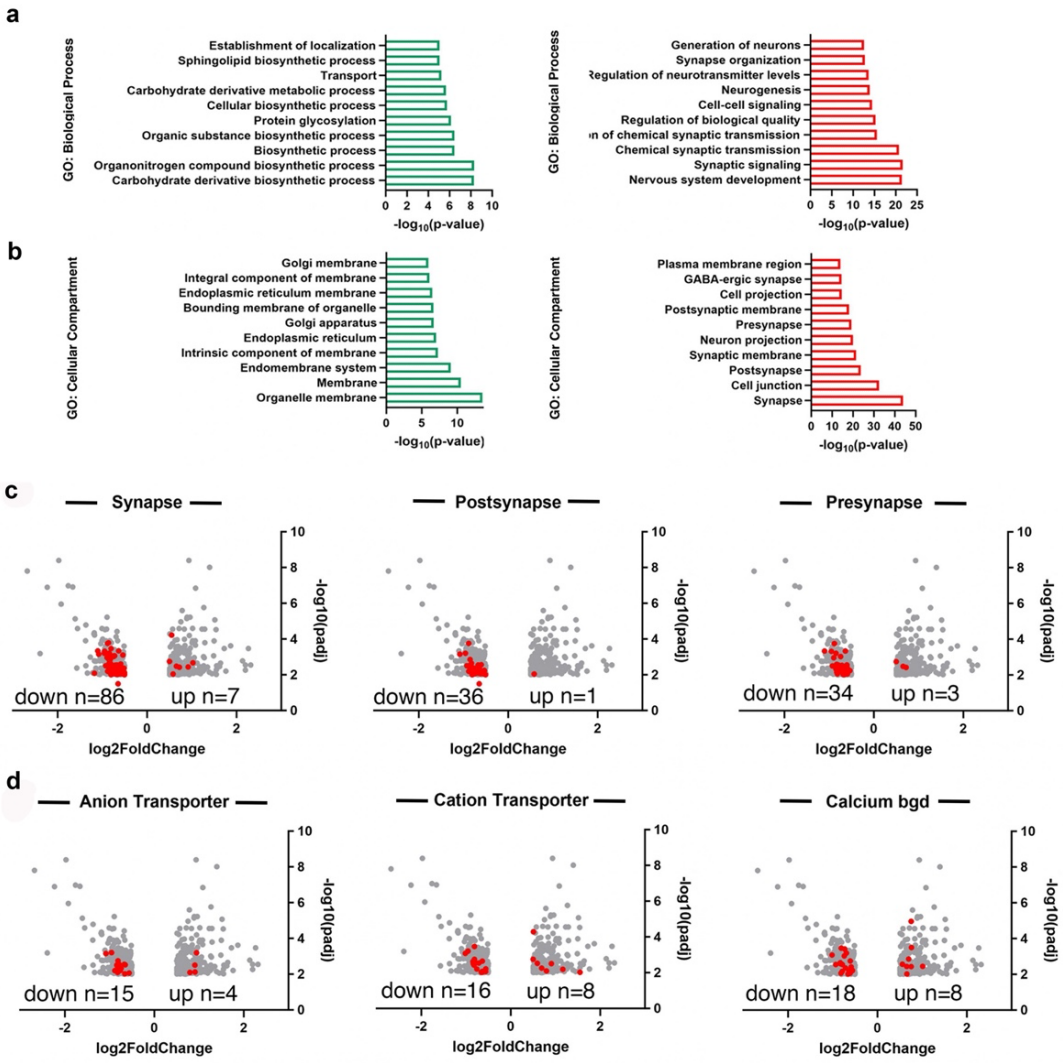

Figure 6: *Trans-synaptic changes after Panx1a ablation and MPTP treatment.* a,b) Summary of the ten most enriched Gene Ontology Biological Processes and Cellular compartments found in Panx1a$^{+/+MPTP}$ and Panx1a$^{-/-MPTP}$ treated larvae. The P-values of each category represent the false discovery rate presented as inverse log10. c), d) Volcano plots represent the differentially expressed genes in Panx1a$^{+/+MPTP}$ and Panx1a$^{-/-MPTP}$ treated larvae (red dots). Gray dots represent the 671 differentially expressed genes found in both genotypes. The cutoff filter was: log2 >0.5 or <-0,5 and padj <0.01.

609
610 ***Loss-of-Panx1a function alters the power of theta, beta- and gamma-waves in the optic tectum.***

611 The impact of MPTP-induced cell death and alterations in energy metabolism on brain
612 activity was assessed by Local Field Potential (LFP) recordings. We determined how the absence
613 of Panx1a influenced local neuronal circuits following acute MPTP treatment by strategically
614 positioned electrodes in the optic tectum (OT) and dorsomedial forebrain (DM), regions
615 previously identified as having cell loss after exposure to 10µM MPTP **(Fig. 7a).** Simultaneous
616 recordings of brain waves were performed on awake, immobilized 6dpf larvae. We categorized
617 frequency spectra into specific bands (Theta: 3.5-7.5Hz, Beta: 12-30Hz, Gamma: 35-45Hz),
618 employing a common approach used in mammalian electrophysiological data analysis that is
619 applicable to zebrafish. Raw traces **(Fig. 7b)** underwent lowpass filtering (<300Hz) to isolate
620 Theta, Beta, and Gamma waves **(Fig. 7c,d).** Our LFP analysis focused on computing Power
621 Spectra Densities (PSDs) at these frequencies, with ranges selected from human brain wave
622 investigation.

623 Significant inverse relationships were observed for theta, beta, and gamma power in the
624 OTs of both genotypes (PSD % values: Theta - Panx1a$^{+/+}$ 0.253 vs Panx1a$^{+/+MPTP}$: 0.019, P-value
625 < 0.0001, Panx1a$^{-/-}$: 0.196 vs Panx1a$^{-/-MPTP}$: 0.275, P-value = 0.0052; Beta - Panx1a$^{+/+}$: 0.018 vs
626 Panx1a$^{+/+MPTP}$: 0.011, P-value < 0.0001, Panx1a$^{-/-}$: 0.009 vs Panx1a$^{-/-MPTP}$: 0.024, P-value <
627 0.0001; Gamma - Panx1a$^{+/+}$: 0.227 vs Panx1a$^{+/+MPTP}$: 0.397, P-value = 0.0012, Panx1a$^{-/-}$: 0.145 vs
628 Panx1a$^{-/-MPTP}$: 0.131, P-value = 0.849). Similar trends were observed in the DM following MPTP
629 treatment in both genotypes. PSDs of Panx1a$^{+/+}$ and Panx1$^{-/-}$ larvae either decreased in Panx1a$^{+/+}$
630 (Theta: Panx1a$^{+/+}$: 0.339 vs Panx1a$^{+/+MPTP}$: 0.157, P-value < 0.0001, Panx1a$^{-/-}$: 0.330 vs Panx1a$^{-/-}$
631 ^{MPTP}: 0.231, P-value = 0.188), remained unchanged (Beta: Panx1a$^{+/+}$: 0.016 vs Panx1a$^{+/+MPTP}$:
632 0.015, P-value = 0.660, Panx1a$^{-/-}$: 0.013 vs Panx1a$^{-/-MPTP}$: 0.014, P-value = 0.978), or decreased

633 in Panx1a$^{+/+}$ and increased in Panx1a$^{-/-}$ (Gamma: Panx1a$^{+/+}$: 0.407 vs Panx1a$^{+/+MPTP}$: 0.267, P-
634 value = 0.0465, Panx1a$^{-/-}$: 0.101 vs Panx1a$^{-/-MPTP}$: 0.264, P-value < 0.0001) **(Fig. 7e,f).**

635 We demonstrated that the LFPs in neuronal circuits in the OT and DM regions responded
636 differently to MPTP+ when Panx1a was present. It was concluded that the changes occurring
637 within selected spectral frequency bands connect functions of Panx1 to synaptic plasticity and
638 mammalian CNS circuit pathophysiology.

639 Our findings demonstrate differential responses in LFPs within neuronal circuits of the
640 OT and DM regions to MPTP when Panx1a is present. The observed changes in selected spectral
641 frequency bands suggest a connection between Panx1 functions and synaptic plasticity, shedding
642 light on mammalian CNS circuit pathophysiology.

643

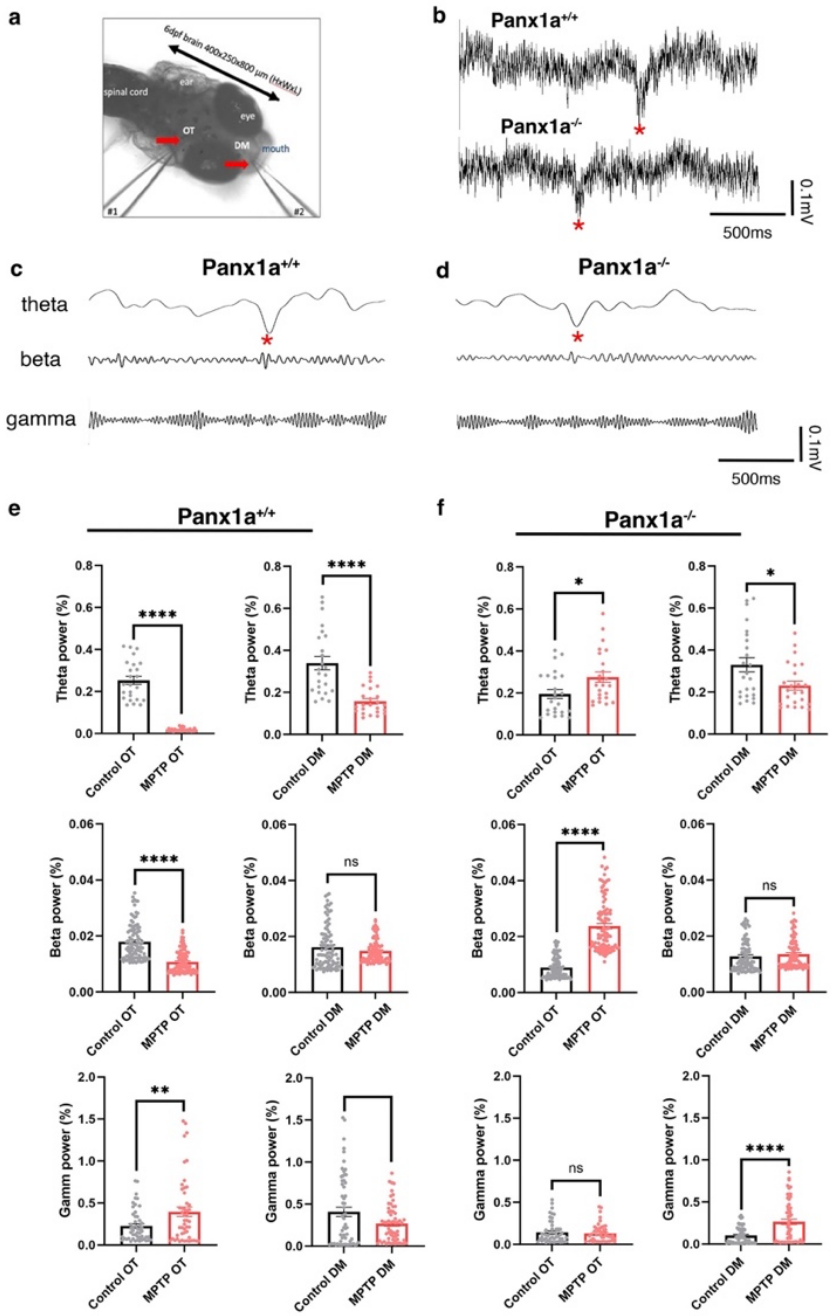

644

645 **Figure 7:** *Loss-of-Panx1a function alters the power of theta, beta- and gamma-waves in the optic*
646 *tectum. a)* Representative image of a two-electrode setup with electrode #1 and electrode#2
647 placed into the optic tectum (OT) and dorsomedial forebrain (DM), respectively. b) Raw
648 recording traces before isolating c,d) theta (3.5 – 7Hz), beta (12 -30Hz), and low gamma-wave
649 (35 – 45Hz) frequency ranges. The red star indicates a reference point in the traces. e,f)
650 Comparisons of the theta, beta, and gamma-power of Panx1a$^{+/+}$ and Panx1a$^{-/-}$ larvae without
651 (control) and with 10µM MPTP treatment. Statistical approach: Outliers were removed using a
652 ROUT test (Q = 1%). Significance was calculated using a Welch's t-test. Number of larvae, n = 8
653 for Panx1a$^{+/+}$ and Panx1a$^{-/-}$. Mean ± SEM. Statistical significance was indicated as *: P-values *
654 <0.05, ** <0.01, *** <0.005, **** <0.001, ns = not significant.

655 ***Loss-of-Panx1a reverses the coherence of local field potentials.***

656 A coherence analysis of LFPs in the frequency range from 0 to 60hz tested the impact of
657 Panx1a ablation and MPTP treatment on the connectivity between the OT and DM, two pivotal
658 regions in the ascending visual pathway **(Fig. 8a).** The zebrafish ascending visual pathway
659 comprises polysynaptic connections, with retinal input to the OT and subsequent projections from
660 the OT to the lateral preglomerular complex and the pallium, including the DM [15,16].

661 MPTP treatment caused a reduction in coherence between OT and DM in Panx1a$^{+/+}$ larvae
662 across theta (Panx1a$^{+/+}$: 0.764, Panx1a$^{+/+MPTP}$: 0.470, P-value < 0.0001) and beta frequencies
663 (Panx1a$^{+/+}$: 0.650, Panx1a$^{+/+MPTP}$: 0.425, P-value < 0.0001) **(Fig. 8b,c)**. Panx1a$^{-/-}$ larvae exhibited
664 the converse effect, with augmented coherence in theta (Panx1a$^{-/-}$: 0.523, Panx1a$^{-/-MPTP}$: 0.469, P-
665 value < 0.0001) and beta frequencies (Panx1a$^{-/-}$: 0.330, Panx1a$^{-/-MPTP}$: 0.490, P-value < 0.0001).
666 Prior investigations have associated elevated beta frequency coherence with Parkinson's disease
667 pathology [17]. The potential ramifications of the observed beta frequency coherence increase in
668 Panx1a$^{-/-}$ larvae warranted further exploration. Furthermore, Panx1a$^{+/+}$ larvae demonstrated a
669 notable increase in low gamma coherence (Panx1a$^{+/+}$: 0.525, Panx1a$^{+/+MPTP}$: 0.612, P-value
670 0.0001), a phenomenon previously linked to uncertainty [18].

671 Collectively, alterations in theta, beta, and low gamma coherence in Panx1a$^{+/+}$ larvae
672 suggested that MPTP treatment induced a functional modulation of neural network mechanisms,
673 likely involving a combination of loss of cell homeostasis, synaptic plasticity, and cell death.

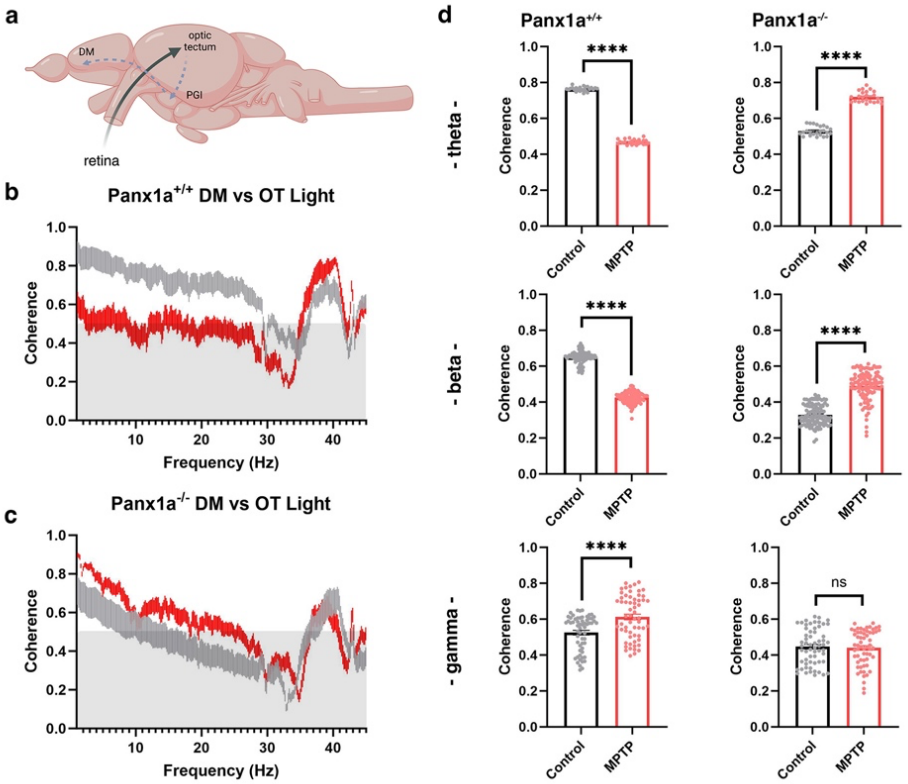

674

675 **Figure 8.** *Loss-of-Panx1a function reverses the coherence of local field potentials. a)* Outline of
676 the ascending visual pathway. b,c) Shows the coherence of local field potentials measured in the
677 optic tectum (OT) and the dorso-medial forebrain (DM) of 6dpf Panx1a$^{+/+}$ and Panx1a$^{-/-}$ larvae.
678 The traces represent the 95% confidence intervals (CI) without (in grey) and after 4hrs of
679 treatment with 50µM MPTP (in red). d) The theta (3.5 – 7Hz), beta (12 -30Hz) and gamma-
680 waves (35 – 45Hz) coherence without (control, in grey) and after MPTP treatment (in red).
681 Statistical approach: Outliers were removed using a ROUT test (Q = 1%). Significance was
682 calculated using a Welch's t-test. Number of larvae, n = 8 for Panx1a$^{+/+}$ and Panx1a$^{-/-}$.
683 Mean ± SEM. Statistical significance was indicated as *: P-values * <0.05, ** <0.01, ***<0.005,
684 **** < 0.001, ns= not significant.
685

686

687 ***Discussion***

688 In this study acute MPTP-induced neurotoxicity served as a model to study Panx1a function in a

689 period of zebrafish neurodevelopment that is considered to resemble late-term to birth in

690 Mammalia. The principal results provide insights into how Panx1a affects the complex

691 mechanisms of metabolic stress, including oxidative stress, mitochondrial dysfunction, and

692 altered synaptic plasticity, thereby making inroads into the metabolic and synaptic aspects of
693 neurodevelopmental and neurodegenerative diseases. Collectively we introduce a first-hand
694 perspective on the role of Panx1a channels in the context of acute MPTP-induced changes of
695 mitochondrial health in dopaminergic neurons; the evidence supports a role of Panx1a in
696 regulating complex cell communication and signaling pathways required for the maintenance of
697 neuronal homeostasis and network functions.
698
699 ***Panx1a mediates neuronal homeostasis via AMPK-pathway activation and mTOR signaling.***
700 The upregulation of mitochondrial Complex I and III genes in Panx1a-deficient and
701 MPTP treated larvae indicates significant changes in mitochondrial homeostasis. These changes
702 are associated with pathways leading to hypoxia, reactive oxygen species (ROS) production,
703 glucose and fatty acid metabolism, or the unfolded protein response, underscoring the necessity
704 of Panx1a for maintaining metabolic and energetic balance *in vivo*.
705 Although the direct functions of Panx1 in mitochondrial health in the nervous system are
706 not fully understood, Panx1a likely operates akin to a "rheostat." In this concept, Panx1 channels
707 open and close in response to varying brain states, with ATP and calcium concentration dynamics
708 serving as messengers of these states. The known structural aspects of Panx1 proteins, such as
709 functioning as a large pore ATP release channel or a narrow Cl channel [19,20], interacting with
710 different lipid environments [21], or interacting proteins [22], could be contributing to a rheostat
711 function.
712 The regulation of the AMP-activated protein kinase (AMPK) pathway showed the
713 activation of a crucial cellular energy sensor to maintain energy homeostasis [23]. AMPK is
714 activated in response to an increase in the AMP/ATP ratio, which occurs during cellular stress or
715 energy depletion [24]. We identified both ATP depletion and the differential expression of subunits

716 of the zebrafish AMPK in both genotypes after MPTP treatment suggesting simultaneous loss of
717 Panx1-mediated ATP release and depletion of ATP after Complex I blocking can activate AMPK
718 to enhance alternative energy production pathways.

719 Alternative catabolic pathways like the observed transcriptional activation of glycolysis
720 and fatty acid metabolism help to restore the energy balance by inhibiting anabolic processes and
721 while stimulating catabolic pathways [25] However, prolonged ATP depletion can trigger
722 endoplasmic reticulum (ER) stress, initiating the unfolded protein response (UPR) [26]. While the
723 UPR seeks to restore protein homeostasis, severe or persistent ER and mitochondrial stress can
724 activate apoptotic pathway [27]. Interestingly, activation of Pannexin-1 and AMPK signaling
725 pathway in the cerebral cortex of a mouse model of Sepsis-associated encephalopathy (SAE) was
726 coupled with the activation of pyroptosis, a highly inflammatory form of lytic programmed cell
727 death, and the incomplete activation of autophagy, which breaks down and recycles old,
728 damaged, or abnormal proteins, especially during periods of stress or starvation [28]. In contrast,
729 the inhibition of pannexin-1 expression reduced the rates of mortality and the cortical
730 pathological changes in the mice, further stimulating the AMPK signaling pathway, inhibiting
731 pyroptosis, and activating autophagy [28]. Here, we observed an up-regulation of autophagy and
732 apoptosis related genes but no differential expression of GasderminD/E expression, a hallmark of
733 pyroptosis, was not detected. This observation supports a theory that by targeting Panx1 in mice
734 and fish inflammation caused by neuronal pyroptosis can be regulated through autophagy
735 activation by the AMPK signaling pathway.

736 In Panx1a$^{-/-MPTP}$ larvae, intensified cell death via autophagy seems to represent an exit
737 strategy in response to disturbed neuronal homeostasis and mitochondrial health. Our data
738 implicate specific cell death pathways, notably those involving the mammalian target of
739 rapamycin complex 1 (mTORC1). In general, mTOR regulates various cellular functions such as

740 protein synthesis, energy metabolism, cell size, lipid metabolism, autophagy, and lysosome
741 biogenesis [29]. The mTOR-controlled signaling pathways are crucial for neuronal development,
742 synaptic plasticity, memory storage, and cognition [30]. Dysregulation of mTOR signaling is a
743 common feature of neurological and neuropsychiatric disorders. Mutations in synaptic genes and
744 mitochondrial perturbation is increasingly recognized as a significant driver of synaptic
745 dysfunction in autism spectrum disorder (ASD) [31]. Individuals with ASD often show deficits in
746 mitochondrial oxidative phosphorylation, linking mitochondrial dysfunction to the disorder's
747 development [32]. Recent research has highlighted the significant roles of AMP-activated protein
748 kinase (AMPK) and the mammalian target of rapamycin (mTOR) signaling pathways in the
749 pathogenesis of ASD [33]. Genetic mutations in regulators of mTOR, such as TSC1, TSC2, and
750 PTEN, have been associated with ASD-like phenotypes, suggesting that mTOR dysregulation
751 contributes to the disorder's development. Moreover, the PI3K/Akt/mTOR pathway's
752 overactivation during brain development can lead to increased cell death, neuroinflammation, and
753 oxidative stress, further exacerbating ASD symptoms [33]. AMPK, a key energy sensor in cells,
754 interacts with the mTOR pathway, and its overactivation has been shown to suppress mTOR
755 signaling, leading to defects in dendritic morphology and increased susceptibility to anxiety,
756 which is often comorbid with ASD [34]. Overall, the AMPK and mTOR pathways are crucial in the
757 neurodevelopmental processes underlying ASD. Interestingly, two studies recently linked Panx1
758 to ASD; ASD susceptibility genes were found in the murine Panx1 interactome, and loss of
759 Panx1 changes social behaviors in an experimental model for early-life seizures [22,35].
760
761 ***Panx1a modulates the molecular composition and bioelectrical function of synapses.***
762 Information about Panx1's involvement in transsynaptic activities and synapse organization
763 was found in the differential expression of genes encoding proteins with pre- and postsynaptic

764 localization in metabolically challenged zebrafish. The expression changes include the
765 downregulation of the presynaptic SNARE complex, postsynaptic excitatory ionotropic AMPA-,
766 NMDA-, and kainite receptors subunits, inhibitory GABA-gated chloride ion channel, or anion and
767 cation channels. Other molecular changes include the downregulation of biomarkers affecting
768 neuronal homeostasis, synapse function, and axonal processes. The downregulation of genes
769 encoding both pre- and postsynaptic proteins suggest trans-synaptic functions of Panx1's function
770 associated with synaptic homeostasis in both excitatory and inhibitory neurons.

771 In 2007, we have postulated that Panx1 channel localization in postsynaptic contacts of
772 mouse cerebral cortex and the hippocampus represents a strategic position for synapse function
773 modulation [36]. Our group and others later demonstrated that loss of murine Panx1 channels causes
774 enhanced and functional modifications of synapses encompassing increased hippocampal
775 excitability, complex dendritic branching, enhanced spine maturation, and an increased proportion
776 of multiple synaptic contacts in hippocampal neurons of Panx1-KO mice [37-39]. Further, Panx1-
777 mediated currents were potentiated by metabotropic receptors and bidirectionally modulated by
778 burst-timing-dependent plasticity of NMDAR-mediated transmission [40]. Moreover, under genetic
779 conditions associated with neurodegenerative disorders (NDDs), suppression of Panx1 can restore
780 synaptic plasticity. For example, in a transgenic Alzheimer's Disease model, pharmacological
781 blocking of Panx1 significantly reduced excitatory synaptic defects by normalizing long-term
782 potentiation (LTP) and depression (LTD) and improving dendritic arborization and spine density
783 in hippocampal neurons [41]. Genetic ablation of Panx1 suggested that Panx1 negatively regulated
784 cortical dendritic spines development [42]. In the visual system, Panx1 channels contribute to the
785 synaptic modulation of a horizontal cell to a photoreceptor feedback mechanism in the horizontal
786 cell dendrites of the mouse and the zebrafish [43-45]. Furthermore, loss of Panx1 caused altered

787 learning and memory in mice such as diminished cognitive functions including altered spatial
788 reference memory, or spatial reversal learning [37,39,46,47].

789 Despite accumulating evidence for the roles of Panx1 in synaptic plasticity, mechanistic
790 details of the cellular processes and molecular pathways have been emerging slowly.
791 Internalization of Panx1 by ATP and P2X7-dependent endocytosis and degradation [48,49] and
792 suppression of presynaptic glutamate release via NMDA receptors and Panx1 have been reported
793 [50]. Panx1 coupling to NMDA receptor functions via Src [51], STIM1/2 [52] or actin, and Rho GTPases,
794 appear to be relevant for synapse stability [38]. Panx1 channel blockage with the mimetic peptide
795 [10]Panx1 increases the synaptic level of endocannabinoids (eCB) and the activation of cannabinoid
796 receptors type 1 (CB1Rs), decreasing hippocampal GABAergic efficacy and shifting
797 excitation/inhibition (E/I) balance toward excitation and facilitating the induction of long-term
798 potentiation [53]. Further, we have reported a pathway that connects NMDA receptor signaling to the
799 opening of electrical synapse protein Cx36 via Panx1 and CaMK2a, suggesting the active
800 participation of Panx1 in modulating both chemical and electrical synapse function by using a
801 shared molecular machinery [54].

802 Jointly, the new discoveries support Panx1's crucial role in cell communication and
803 signaling processes in neurons, emphasizing an association with synaptic stability, memory
804 formation, and intercellular signaling. Here, we demonstrated that Panx1a ablation influenced local
805 field potential power of theta, beta, and gamma waves in the optic tectum and dorsomedial
806 forebrain. This result implies a correlation between metabolic changes and synapse functions
807 providing insights into how Panx1a deficiency alters brain wave activity and neuronal circuit
808 responses. The modulation of coherence is evidence that the loss of Panx1a leads to changes in the
809 relationship of the different brain regions across various frequency bands. Together, the findings
810 of the LFP analysis establish a link between Panx1a functions and synaptic plasticity within

811 neuronal circuits, supporting a role of Panx1a in maintaining synaptic stability and modulating
812 brain activity ultimately correlating changes of brain function with the differential expression of
813 pre-and postsynaptic genes.

814 The results fill a gap in understanding how Panx1a affects neural network connectivity and
815 information processing, offering insight into Panx1's role in disease pathology. Indeed, local field
816 potentials (LFPs) can be altered in neurodevelopmental disorders. In autism spectrum disorder
817 (ASD), mice prenatally exposed to valproic acid (VPA) exhibited significant changes in LFPs
818 across several brain regions [55]. These mice showed increased low gamma activity in the
819 hippocampus during awake immobility and altered theta oscillations correlated with locomotor
820 speed, which were not observed in control mice. Additionally, increased delta and beta activities
821 were found in the olfactory bulb during different states of activity, along with altered coherence
822 between the hippocampus and both the olfactory bulb and medial prefrontal cortex, suggesting
823 disrupted neural signaling in learning-related brain areas [55]. Notably, LFPs reflect the activity of
824 spatially localized populations of neurons, and alterations in LFP activity can be indicative of
825 cognitive processes, such as attention, which may be disrupted in neurodevelopmental disorders.

826 Local field potentials (LFPs) are also altered in neurodegenerative disorders, reflecting
827 changes in neural network activities and brain connectivity. In Alzheimer's disease (AD), studies
828 on APP/PS1 mice models have shown that the LFPs in the gamma band of the left and right
829 secondary motor cortex (M2) are more synchronized compared to wild-type controls, indicating a
830 decline in hemispheric asymmetry, which could be an early sign of AD [56]. Similarly, in Parkinson's
831 disease (PD), alterations in LFPs have been observed in several brain regions [57]. Beyond AD and
832 PD, LFP alterations have also been noted in psychiatric conditions like major depressive disorder
833 (MDD) and obsessive-compulsive disorder (OCD) [58,59]. These studies have found that different

834 frequency bands are associated with specific symptoms, with low-frequency activity closely related
835 to OCD symptoms, while LFP findings in MDD are more complex and varied [60 61].
836
837 **Conclusion**
838 Overall, we show that Panx1a is crucial for neuronal viability by regulating energy
839 metabolism, facilitating cellular communication, and maintaining synaptic homeostasis. Our
840 research identifies the AMPK-mTORC1 pathway as a key regulator of processes activating cell
841 death pathways that allow the orderly degradation and recycling of cellular components. We
842 propose that the evidence strongly suggests that Panx1a acts as a safeguard for neuronal health by
843 modulating ATP signaling, thereby preserving metabolic and energetic homeostasis. The critical
844 role of Panx1a in regulating synaptic plasticity and neuronal homeostasis, is likely impacting
845 neuropsychiatric disorders like autism spectrum disorder (ASD) or early in life disturbances
846 leading to neurodegenerative disorders like Alzheimer's or Parkinson's disease.
847
848
849
850
851
852
853
854
855 **Acknowledgements.** We thank two members of York University Zebrafish Vivarium, Janet
856 Fleites-Medina, and Veronica Scavo for outstanding zebrafish husbandry. We also wish to thank
857 the Center for Applied Genomics, SickKids, Toronto, ON, Canada for the RNA-seq service.
858

Funding. This research was supported by the Natural Sciences and Engineering Research Council (NSERC) discovery grant RGPIN-2019-06378 (GRZ).

Author contributions. Conceptualization, GSZ, GRZ; data analysis, GSZ, NS, GRZ; investigation, GSZ, NS, CZ; writing—original draft preparation, GSZ, GRZ; writing—review and editing, all authors; visualization, GSZ, NS, GRZ; supervision, SC, GRZ; project administration, GRZ; funding acquisition, GRZ.

Consent for publication. All authors have read and agreed to the published version of the manuscript.

Ethics approval: All animal work was performed at York University's zebrafish vivarium and in an S2 biosafety laboratory following the Canadian Council for Animal Care guidelines after approval of the study protocol by the York University Animal Care Committee (GZ#2019-7-R2).

Data Availability. The RNA-seq data are deposited at the NCBI - Gene Expression Omnibus (GEO) database repository (ID pending at time of submission). Additional information necessary for the reanalysis of the data reported in this manuscript is available from the corresponding author upon request.

Competing interests. The authors declare no competing interests.

Materials & Correspondence. Correspondence and material requests should be addressed to Georg R. Zoidl.

Abbreviations

Gene IDs follow ZFIN Zebrafish Nomenclature standards:
https://zfin.atlassian.net/wiki/spaces/general/pages/1818394635/ZFIN+Zebrafish+Nomenclature+Conventions

AD: Alzheimer's Disease
ALS: Amyotrophic lateral sclerosis
AMPA: α-amino-3-hydroxy-5-methyl-4-isoxazolepropionic acid

AO: Acridine-Orange
ATP: Adenosine triphosphate
CNS: Central nervous system
DM: Dorsomedial pallium (amygdala)
DGE: differential gene expression
dpf: days post fertilization
FDR: False discovery rate
FFT: fast Fourier transform
Fps: frames per second
GABA: γ-Aminobutyric acid
GEO: Gene expression omnibus
GO: Gene Ontology
GSEA: Gene set enrichment analysis
HD: Huntington's Disease
KEGG: Kyoto Encyclopedia of Genes and Genomes
LFP: Local field potential
NMDA: N-Methyl-D-aspartic acid
MSigDB: Molecular Signatures Database
MPTP: 1-methyl-4-phenyl-1,2,3,6-tetrahydropyridine
NDD: neurodegenerative disorder
OT: Optic tectum
Padj: adjusted P-value
Panc: Pancuronium bromide
PD: Parkinson's Disease
PCA: Principal component analysis
PSD: Power spectral density
PROBS: Phosphate-Buffered Saline
ROS: Reactive oxygen species
RNA-seq: RNA sequencing
SEM: standard error of the mean
SNARE: soluble N-ethylmaleimide-sensitive fusion protein attachment protein receptors
TL: Tubingen longfin
UPR: Unfolded protein response
ZFIN: Zebrafish Information Network

References

1 Safarian, N., Whyte-Fagundes, P., Zoidl, C., Grigull, J. & Zoidl, G. Visuomotor deficiency in panx1a knockout zebrafish is linked to dopaminergic signaling. *Sci Rep* **10**, 9538 (2020). https://doi.org/10.1038/s41598-020-66378-y

2 Safarian N., H.-T. S., Zoidl C., Zoidl G.R. Panx1b modulates the luminance response and direction of motion in the zebrafish. *BioRxiv* **BIORXIV-2021-453251v1-Zoidl** (2021).

3 Safarian, N., Houshangi-Tabrizi, S., Zoidl, C., & Zoidl, G.R. . Panx1b Modulates the Luminance Response and Direction of Locomotion in the Zebrafish. *Int. J. Mol. Sci.* (2021). https://doi.org/https://doi.org/10.3390/ijms222111750

4 MacPhail, R. C. *et al.* Locomotion in larval zebrafish: Influence of time of day, lighting and ethanol. *Neurotoxicology* **30**, 52-58 (2009). https://doi.org/10.1016/j.neuro.2008.09.011

5 Safarian, N., Houshangi-Tabrizi, S., Zoidl, C. & Zoidl, G. R. Panx1b Modulates the Luminance Response and Direction of Locomotion in the Zebrafish. *Int J Mol Sci* **22** (2021). https://doi.org/10.3390/ijms222111750

6 Baraban, S. C. Forebrain electrophysiological recording in larval zebrafish. *J Vis Exp* (2013). https://doi.org/10.3791/50104

7 Whyte-Fagundes, P. *et al.* A Potential Compensatory Role of Panx3 in the VNO of a Panx1 Knock Out Mouse Model. *Front Mol Neurosci* **11**, 135 (2018). https://doi.org/10.3389/fnmol.2018.00135

8 McCarthy, D. J., Chen, Y. & Smyth, G. K. Differential expression analysis of multifactor RNA-Seq experiments with respect to biological variation. *Nucleic Acids Res* **40**, 4288-4297 (2012). https://doi.org/10.1093/nar/gks042

9 Robinson, M. D., McCarthy, D. J. & Smyth, G. K. edgeR: a Bioconductor package for differential expression analysis of digital gene expression data. *Bioinformatics* **26**, 139-140 (2010). https://doi.org/10.1093/bioinformatics/btp616

10 Abad Tan, S., Zoidl, G. & Ghafar-Zadeh, E. A Multidisciplinary Approach Toward High Throughput Label-Free Cytotoxicity Monitoring of Superparamagnetic Iron Oxide Nanoparticles. *Bioengineering (Basel)* **6** (2019). https://doi.org/10.3390/bioengineering6020052

11 Seal, R. L. *et al.* Genenames.org: the HGNC resources in 2023. *Nucleic Acids Res* **51**, D1003-D1009 (2023). https://doi.org/10.1093/nar/gkac888

12 Mudunuri, U., Che, A., Yi, M. & Stephens, R. M. bioDBnet: the biological database network. *Bioinformatics* **25**, 555-556 (2009). https://doi.org/10.1093/bioinformatics/btn654

13 Ray, A., Zoidl, G., Weickert, S., Wahle, P. & Dermietzel, R. Site-specific and developmental expression of pannexin1 in the mouse nervous system. *Eur J Neurosci* **21**, 3277-3290 (2005). https://doi.org/10.1111/j.1460-9568.2005.04139.x

14 Subramanian, A. *et al.* Gene set enrichment analysis: a knowledge-based approach for interpreting genome-wide expression profiles. *Proc Natl Acad Sci U S A* **102**, 15545-15550 (2005). https://doi.org/10.1073/pnas.0506580102

15 Bloch, S. *et al.* Non-thalamic origin of zebrafish sensory nuclei implies convergent evolution of visual pathways in amniotes and teleosts. *Elife* **9** (2020). https://doi.org/10.7554/eLife.54945

16 Mueller, T. What is the Thalamus in Zebrafish? *Front Neurosci* **6**, 64 (2012). https://doi.org/10.3389/fnins.2012.00064

17 Asadi, A., Madadi Asl, M., Vahabie, A. H. & Valizadeh, A. The Origin of Abnormal Beta Oscillations in the Parkinsonian Corticobasal Ganglia Circuits. *Parkinsons Dis* **2022**, 7524066 (2022). https://doi.org/10.1155/2022/7524066

18 Nurislamova, Y. M., Novikov, N. A., Zhozhikashvili, N. A. & Chernyshev, B. V. Enhanced Theta-Band Coherence Between Midfrontal and Posterior Parietal Areas Reflects Post-

feedback Adjustments in the State of Outcome Uncertainty. *Front Integr Neurosci* **13**, 14 (2019). https://doi.org/10.3389/fnint.2019.00014

19 Dahl, G. The Pannexin1 membrane channel: distinct conformations and functions. *FEBS Lett* **592**, 3201-3209 (2018). https://doi.org/10.1002/1873-3468.13115

20 Mim, C., Perkins, G. & Dahl, G. Structure versus function: Are new conformations of pannexin 1 yet to be resolved? *J Gen Physiol* **153** (2021). https://doi.org/10.1085/jgp.202012754

21 Anderson, C. L. & Thompson, R. J. Intrapore lipids hydrophobically gate pannexin-1 channels. *Sci Signal* **15**, eabn2081 (2022). https://doi.org/10.1126/scisignal.abn2081

22 Frederiksen, S. D., Wicki-Stordeur, L. E. & Swayne, L. A. Overlap in synaptic neurological condition susceptibility pathways and the neural pannexin 1 interactome revealed by bioinformatics analyses. *Channels (Austin)* **17**, 2253102 (2023). https://doi.org/10.1080/19336950.2023.2253102

23 Muraleedharan, R. & Dasgupta, B. AMPK in the brain: its roles in glucose and neural metabolism. *FEBS J* **289**, 2247-2262 (2022). https://doi.org/10.1111/febs.16151

24 Steinberg, G. R. & Hardie, D. G. New insights into activation and function of the AMPK. *Nat Rev Mol Cell Biol* **24**, 255-272 (2023). https://doi.org/10.1038/s41580-022-00547-x

25 Athari, S. Z., Farajdokht, F., Keyhanmanesh, R. & Mohaddes, G. AMPK Signaling Pathway as a Potential Therapeutic Target for Parkinson's Disease. *Adv Pharm Bull* **14**, 120-131 (2024). https://doi.org/10.34172/apb.2024.013

26 Volgyi, K., Juhasz, G., Kovacs, Z. & Penke, B. Dysfunction of Endoplasmic Reticulum (ER) and Mitochondria (MT) in Alzheimer's Disease: The Role of the ER-MT Cross-Talk. *Curr Alzheimer Res* **12**, 655-672 (2015). https://doi.org/10.2174/1567205012666150710095035

27 Ekundayo, B. E. *et al.* Oxidative Stress, Endoplasmic Reticulum Stress and Apoptosis in the Pathology of Alzheimer's Disease. *Cell Biochem Biophys* **82**, 457-477 (2024). https://doi.org/10.1007/s12013-024-01248-2

28 Lei, Y. *et al.* The pannexin-1 channel regulates pyroptosis through autophagy in a mouse model of sepsis-associated encephalopathy. *Ann Transl Med* **9**, 1802 (2021). https://doi.org/10.21037/atm-21-6579

29 Panwar, V. *et al.* Multifaceted role of mTOR (mammalian target of rapamycin) signaling pathway in human health and disease. *Signal Transduct Target Ther* **8**, 375 (2023). https://doi.org/10.1038/s41392-023-01608-z

30 Bockaert, J. & Marin, P. mTOR in Brain Physiology and Pathologies. *Physiol Rev* **95**, 1157-1187 (2015). https://doi.org/10.1152/physrev.00038.2014

31 Rojas-Charry, L., Nardi, L., Methner, A. & Schmeisser, M. J. Abnormalities of synaptic mitochondria in autism spectrum disorder and related neurodevelopmental disorders. *J Mol Med (Berl)* **99**, 161-178 (2021). https://doi.org/10.1007/s00109-020-02018-2

32 Khaliulin, I., Hamoudi, W. & Amal, H. The multifaceted role of mitochondria in autism spectrum disorder. *Mol Psychiatry* (2024). https://doi.org/10.1038/s41380-024-02725-z

33 Thomas, S. D., Jha, N. K., Ojha, S. & Sadek, B. mTOR Signaling Disruption and Its Association with the Development of Autism Spectrum Disorder. *Molecules* **28** (2023). https://doi.org/10.3390/molecules28041889

34 Ma, J. *et al.* Dysregulation of AMPK-mTOR signaling leads to comorbid anxiety in Dip2a KO mice. *Cereb Cortex* **33**, 4977-4989 (2023). https://doi.org/10.1093/cercor/bhac393

35 Obot, P. *et al.* Pannexin1 Mediates Early-Life Seizure-Induced Social Behavior Deficits. *ASN Neuro* **16**, 2371164 (2024). https://doi.org/10.1080/17590914.2024.2371164

36 Zoidl, G. *et al.* Localization of the pannexin1 protein at postsynaptic sites in the cerebral cortex and hippocampus. *Neuroscience* **146**, 9-16 (2007). https://doi.org/10.1016/j.neuroscience.2007.01.061

37 Ardiles, A. O. *et al.* Pannexin 1 regulates bidirectional hippocampal synaptic plasticity in adult mice. *Front Cell Neurosci* **8**, 326 (2014). https://doi.org/10.3389/fncel.2014.00326

38 Flores-Munoz, C. *et al.* The Long-Term Pannexin 1 Ablation Produces Structural and Functional Modifications in Hippocampal Neurons. *Cells* **11** (2022). https://doi.org/10.3390/cells11223646

39 Prochnow, N. *et al.* Pannexin1 stabilizes synaptic plasticity and is needed for learning. *PLoS One* **7**, e51767 (2012). https://doi.org/10.1371/journal.pone.0051767

40 Rangel-Sandoval, C., Soula, M., Li, W. P., Castillo, P. E. & Hunt, D. L. NMDAR-mediated activation of pannexin1 channels contributes to the detonator properties of hippocampal mossy fiber synapses. *iScience* **27**, 109681 (2024). https://doi.org/10.1016/j.isci.2024.109681

41 Flores-Munoz, C. *et al.* Acute Pannexin 1 Blockade Mitigates Early Synaptic Plasticity Defects in a Mouse Model of Alzheimer's Disease. *Front Cell Neurosci* **14**, 46 (2020). https://doi.org/10.3389/fncel.2020.00046

42 Sanchez-Arias, J. C. *et al.* Pannexin 1 Regulates Network Ensembles and Dendritic Spine Development in Cortical Neurons. *eNeuro* **6** (2019). https://doi.org/10.1523/ENEURO.0503-18.2019

43 Vroman, R. *et al.* Extracellular ATP hydrolysis inhibits synaptic transmission by increasing ph buffering in the synaptic cleft. *PLoS Biol* **12**, e1001864 (2014). https://doi.org/10.1371/journal.pbio.1001864

44 Kranz, K. *et al.* Expression of Pannexin1 in the outer plexiform layer of the mouse retina and physiological impact of its knockout. *J Comp Neurol* **521**, 1119-1135 (2013). https://doi.org/10.1002/cne.23223

45 Cenedese, V. *et al.* Pannexin 1 Is Critically Involved in Feedback from Horizontal Cells to Cones. *Front Mol Neurosci* **10**, 403 (2017). https://doi.org/10.3389/fnmol.2017.00403

46 Gajardo, I. *et al.* Lack of Pannexin 1 Alters Synaptic GluN2 Subunit Composition and Spatial Reversal Learning in Mice. *Front Mol Neurosci* **11**, 114 (2018). https://doi.org/10.3389/fnmol.2018.00114

47 Obot, P. *et al.* Astrocyte and Neuronal Panx1 Support Long-Term Reference Memory in Mice. *ASN Neuro* **15**, 17590914231184712 (2023). https://doi.org/10.1177/17590914231184712

48 Boyce, A. K., Kim, M. S., Wicki-Stordeur, L. E. & Swayne, L. A. ATP stimulates pannexin 1 internalization to endosomal compartments. *Biochem J* **470**, 319-330 (2015). https://doi.org/10.1042/BJ20141551

49 Boyce, A. K. J. & Swayne, L. A. P2X7 receptor cross-talk regulates ATP-induced pannexin 1 internalization. *Biochem J* **474**, 2133-2144 (2017). https://doi.org/10.1042/BCJ20170257

50 Bialecki, J. *et al.* Suppression of Presynaptic Glutamate Release by Postsynaptic Metabotropic NMDA Receptor Signalling to Pannexin-1. *J Neurosci* **40**, 729-742 (2020). https://doi.org/10.1523/JNEUROSCI.0257-19.2019

1069 51 Weilinger, N. L. *et al.* Metabotropic NMDA receptor signaling couples Src family kinases
1070 to pannexin-1 during excitotoxicity. *Nat Neurosci* **19**, 432-442 (2016).
1071 https://doi.org/10.1038/nn.4236
1072 52 Patil, C. S. *et al.* ER-resident STIM1/2 couples Ca(2+) entry by NMDA receptors to
1073 pannexin-1 activation. *Proc Natl Acad Sci U S A* **119**, e2112870119 (2022).
1074 https://doi.org/10.1073/pnas.2112870119
1075 53 Garcia-Rojas, F. *et al.* Pannexin-1 Modulates Inhibitory Transmission and Hippocampal
1076 Synaptic Plasticity. *Biomolecules* **13** (2023). https://doi.org/10.3390/biom13060887
1077 54 Siu, R. C. F., Kotova, A., Timonina, K., Zoidl, C. & Zoidl, G. R. Convergent NMDA receptor-
1078 Pannexin1 signaling pathways regulate the interaction of CaMKII with Connexin-36.
1079 *Commun Biol* **4**, 702 (2021). https://doi.org/10.1038/s42003-021-02230-x
1080 55 Cheaha, D., Bumrungsri, S., Chatpun, S. & Kumarnsit, E. Characterization of in utero
1081 valproic acid mouse model of autism by local field potential in the hippocampus and the
1082 olfactory bulb. *Neurosci Res* **98**, 28-34 (2015).
1083 https://doi.org/10.1016/j.neures.2015.04.006
1084 56 Chen, Y., Li, M., Zheng, Y. & Yang, L. Evaluation of Hemisphere Lateralization with
1085 Bilateral Local Field Potential Recording in Secondary Motor Cortex of Mice. *J Vis Exp*
1086 (2019). https://doi.org/10.3791/59310
1087 57 Wang, J. *et al.* Network-wide oscillations in the parkinsonian state: alterations in
1088 neuronal activities occur in the premotor cortex in parkinsonian nonhuman primates. *J*
1089 *Neurophysiol* **117**, 2242-2249 (2017). https://doi.org/10.1152/jn.00011.2017
1090 58 Trenado, C. *et al.* Combined Invasive Subcortical and Non-invasive Surface
1091 Neurophysiological Recordings for the Assessment of Cognitive and Emotional Functions
1092 in Humans. *J Vis Exp* (2016). https://doi.org/10.3791/53466
1093 59 Zhang, W., Xiong, B., Wu, Y., Xiao, L. & Wang, W. Local field potentials in major
1094 depressive and obsessive-compulsive disorder: a frequency-based review. *Front*
1095 *Psychiatry* **14**, 1080260 (2023). https://doi.org/10.3389/fpsyt.2023.1080260
1096 60 Mitiureva, D. *et al.* Comparative analysis of resting-state EEG functional connectivity in
1097 depression and obsessive-compulsive disorder. *Psychiatry Res Neuroimaging* **342**,
1098 111828 (2024). https://doi.org/10.1016/j.pscychresns.2024.111828
1099 61 Gimenez, M. *et al.* Brain alterations in low-frequency fluctuations across multiple bands
1100 in obsessive compulsive disorder. *Brain Imaging Behav* **11**, 1690-1706 (2017).
1101 https://doi.org/10.1007/s11682-016-9601-y
1102